NIST Special Publication 260-129

Standard Reference Materials:

Antireflecting-Chromium Linewidth Standard, SRM 473, for Calibration of Optical Microscope Linewidth Measuring Systems

James E. Potzick

Precision Engineering Division
Manufacturing Engineering Laboratory
National Institute of Standards and Technology
Gaithersburg, MD 20899-0001

U.S. DEPARTMENT OF COMMERCE, William M. Daley, Secretary
TECHNOLOGY ADMINISTRATION, Mary L. Good, Under Secretary for Technology
NATIONAL INSTITUTE OF STANDARDS AND TECHNOLOGY, Arati Prabhakar, Director

Issued February 1997

National Institute of Standards and Technology Special Publication 260–129
Natl. Inst. Stand. Technol. Spec. Publ. 260–129, 35 pages (Feb. 1997)
CODEN: NSPUE2

U.S. GOVERNMENT PRINTING OFFICE
WASHINGTON: 1997

For sale by the Superintendent of Documents, U.S. Government Printing Office, Washington, DC 20402–9325

Preface

Standard Reference Materials (SRMs) as defined by the National Institute of Standards and Technology (NIST) are well-characterized materials, produced in quantity and certified for one or more physical or chemical properties. They are used to assure the accuracy and compatibility of measurements throughout the Nation. SRMs are widely used as primary standards in many diverse fields in science, industry, and technology, both within the United States and throughout the world. They are also used extensively in the fields of environmental and clinical analysis. In many applications, traceability of quality control and measurement processes to the national measurement system is carried out through the mechanism and use of SRMs. For many of the Nation's scientists and technologists, it is therefore of more than passing interest to know the details of the measurements made at NIST in arriving at the certified values of the SRMs produced. The NIST Special Publication 260 Series is a series of papers reserved for this purpose.

The 260 Series is dedicated to the dissemination of information on different phases of the preparation, measurement, certification, and use of NIST SRMs. In general, much more detail will be found in these papers than is generally allowed, or desirable, in scientific journal articles. This enables the user to assess the validity and accuracy of the measurement processes employed, to judge the statistical analysis, and to learn details of techniques and methods utilized for work entailing greatest care and accuracy. These papers also should provide sufficient additional information so SRMs can be utilized in new applications in diverse fields not foreseen at the time the SRM was originally issued.

Inquiries concerning the technical content of this paper should be directed to the author(s). Other questions concerned with the availability, delivery, price, and so forth, will receive prompt attention from:

Standard Reference Materials Program
Bldg. 202, Rm. 204
National Institute of Standards and Technology
Gaithersburg, MD 20899
Telephone: (301) 975-6776
FAX: (301) 948-3730

Thomas E. Gills, Chief
Standard Reference Materials Program

OTHER NIST PUBLICATIONS IN THIS SERIES

Trahey, N.M., ed., NIST Standard Reference Materials Catalog 1995-96, NIST Spec. Publ. 260 (1995 Ed.). PB95-232518/AS

Michaelis, R.E., and Wyman, L.L., Standard Reference Materials: Preparation of White Cast Iron Spectrochemical Standards, NBS Misc. Publ. 260-1 (June 1964). COM74-11061**

Michaelis, R.E., Wyman, L.L., and Flitsch, R., Standard Reference Materials: Preparation of NBS Copper-Base Spectrochemical Standards, NBS Misc. Publ. 260-2 (October 1964). COM74-11063**

Michaelis, R.E., Yakowitz, H., and Moore, G.A., Standard Reference Materials: Metallographic Characterization of an NBS Spectrometric Low-Alloy Steel Standard, NBS Misc. Publ. 260-3 (October 1964). COM74-11060**

Hague, J.L., Mears, T.W., and Michaelis, R.E., Standard Reference Materials: Sources of Information, Publ. 260-4 (February 1965). COM74-11059**

Alvarez, R., and Flitsch, R., Standard Reference Materials: Accuracy of Solution X-Ray Spectrometric Analysis of Copper-Base Alloys, NBS Misc. Publ. 260-5 (February 1965). PB168068**

Shultz, J.I., Standard Reference Materials: Methods for the Chemical Analysis of White Cast Iron Standards, NBS Misc. Publ. 260-6 (July 1965). COM74-11068**

Bell, R.K., Standard Reference Materials: Methods for the Chemical Analysis of NBS Copper-Base Spectrochemical Standards, NBS Misc. Publ. 260-7 (October 1965). COM74-11067**

Richmond, M.S., Standard Reference Materials: Analysis of Uranium Concentrates at the National Bureau of Standards, NBS Misc. Publ. 260-8 (December 1965). COM74-11066**

Anspach, S.C., Cavallo, L.M., Garfinkel, S.B., et al., Standard Reference Materials: Half Lives of Materials Used in the Preparation of Standard Reference Materials of Nineteen Radioactive Nuclides Issued by the National Bureau of Standards, NBS Misc. Publ. 260-9 (November 1965). COM74-11065**

Yakowitz, H., Vieth, D.L., Heinrich, K.F.J., et al., Standard Reference Materials: Homogeneity Characterization of NBS Spectrometric Standards II: Cartridge Brass and Low-Alloy Steel, NBS Misc. Publ. 260-10 (December 1965). COM74-11064**

Napolitano, A., and Hawkins, E.G., Standard Reference Materials: Viscosity of Standard Lead-Silica Glass, NBS Misc. Publ. 260-11** (November 1966).

Yakowitz, H., Vieth, D.L., and Michaelis, R.E., Standard Reference Materials: Homogeneity Characterization of NBS Spectrometric Standards III: White Cast Iron and Stainless Steel Powder Compact, NBS Misc. Publ. 260-12 (September 1966).

Spijkerman, J.J., Snediker, D.K., Ruegg, F.C., et al., Standard Reference Materials: Mossbauer Spectroscopy Standard for the Chemical Shift of Iron Compounds, NBS Misc. Publ. 260-13** (July 1967).

Menis, O., and Sterling, J.T., Standard Reference Materials: Determination of Oxygen in Ferrous Materials (SRMs 1090, 1091, 1092), NBS Misc. Publ. 260-14** (September 1966).

Passaglia, E. and Shouse, P.J., Standard Reference Materials: Recommended Method of Use of Standard Light-Sensitive Paper for Calibrating Carbon Arcs Used in Testing Testiles for Colorfastness to Light, NBS Spec. Publ. 260-15 (July 1967). Superseded by SP 260-41.

Yakowitz, H., Michaelis, R.E., and Vieth, D.L., Standard Reference Materials: Homogeneity Characterization of NBS Spectrometric Standards IV: Preparation and Microprobe Characterization of W-20% Mo Alloy Fabricated by Powder Metallurgical Methods, NBS Spec. Publ. 260-16 (January 1969). COM74-11062**

Catanzaro, E.J., Champion, C.E., Garner, E.L., et al., Standard Reference Materials: Boric Acid; Isotopic, and Assay Standard Reference Materials, NBS Spec. Publ. 260-17 (February 1970). PB189457**

Geller, S.B., Mantek, P.A., and Cleveland, N.G., Calibration of NBS Secondary Standards Magnetic Tape Computer Amplitude Reference Amplitude Measurement "Process A," NBS Spec. Publ. 260-18 (November 1969). Superseded by SP 260-29.

Paule, R.C., and Mandel, J., Standard Reference Materials: Analysis of Interlaboratory Measurements on the Vapor Pressure of Gold (Certification of SRM 745). NBS Spec. Publ. 260-19 (January 1970). PB190071**

260-20: Unassigned

Paule, R.C., and Mandel, J., Standard Reference Materials: Analysis of Interlaboratory Measurements on the Vapor Pressures of Cadmium and Silver, NBS Spec. Publ. 260-21 (January 1971). COM74-11359**

Yakowitz, H., Fiori, C.E., and Michaelis, R.E., Standard Reference Materials: Homogeneity Characterization of Fe-3 Si Alloy, NBS Spec. Publ. 260-22 (February 1971). COM74-11357**

Napolitano, A., and Hawkins, E.G., Standard Reference Materials: Viscosity of a Standard Borosilicate Glass, NBS Spec. Publ. 260-23 (December 1970). COM71-00157**

Sappenfield, K.M., Marinenko, G., and Hague, J.L., Standard Reference Materials: Comparison of Redox Standards, NBS Spec. Publ. 260-24 (January 1972). COM72-50058**

Hicho, G.E., Yakowitz, H., Rasberry, S.D., et al., Standard Reference Materials: A Standard Reference Material Containing Nominally Four Percent Austenite, NBS Spec. Publ. 260-25 (February 1971). COM74-11356**

Martin, J.F., Standard Reference Materials: NBS-U.S. Steel Corp. Joint Program for Determining Oxygen and Nitrogen in Steel, NBS Spec. Publ. 260-26 (February 1971). PB 81176620**

Garner, E.L., Machlan, L.A., and Shields, W.R., Standard Reference Materials: Uranium Isotopic Standard Reference Materials, NBS Spec. Publ. 260-27 (April 1971). COM74-11358**

Heinrich, K.F.J., Myklebust, R.L., Rasberry, S.D., et al., Standard Reference Materials: Preparation and Evaluation of SRMs 481 and 482 Gold-Silver and Gold-Copper Alloys for Microanalysis, NBS Spec. Publ. 260-28 (August 1971). COM71-50365**

Geller, S.B., Standard Reference Materials: Calibration of NBS Secondary Standard Magnetic Tape (Computer Amplitude Reference) Using the Reference Tape Amplitude Measurement "Process A-Model 2," NBS Spec. Publ. 260-29 (June 1971). COM71-50282** Supersedes Measurement System in SP 260-18.

Gorozhanina, R.S., Freedman, A.Y., and Shaievitch, A.B., (translated by M.C. Selby), Standard Reference Materials: Standard Samples Issued in the USSR (A Translation from the Russian), NBS Spec. Publ. 260-30 (June 1971). COM71-50283**

Hust, J.G., and Sparks, L.L., Standard Reference Materials: Thermal Conductivity of Electrolytic Iron SRM 734 from 4 to 300 K, NBS Spec. Publ. 260-31 (November 1971). COM71-50563**

Mavrodineanu, R., and Lazar, J.W., Standard Reference Materials: Standard Quartz Cuvettes for High Accuracy Spectrophotometry, NBS Spec. Publ. 260-32 (December 1973).COM74-50018**

Wagner, H.L., Standard Reference Materials: Comparison of Original and Supplemental SRM 705, Narrow Molecular Weight Distribution Polystyrene, NBS Spec. Publ. 260-33 (May 1972). COM72-50526**

Sparks, L.L., and Hust, J.G., Standard Reference Material: Thermoelectric Voltage of Silver-28 Atomic Percent Gold Thermocouple Wire, SRM 733, Verses Common Thermocouple Materials (Between Liquid Helium and Ice Fixed Points), NBS Spec. Publ. 260-34 (April 1972). COM72-50371**

Sparks, L.L., and Hust, J.G., Standard Reference Materials: Thermal Conductivity of Austenitic Stainless Steel, SRM 735 from 5 to 280 K, NBS Spec. Publ. 260-35 (April 1972). COM72-50368**

Cali, J.P., Mandel, J., Moore, L.J., et al., Standard Reference Materials: A Reference Method for the Determination of Calcium in Serum NBS SRM 915, NBS Spec. Publ. 260-36 (May 1972). COM72-50527**

Shultz, J.I., Bell, R.K., Rains, T.C., et al., Standard Reference Materials: Methods of Analysis of NBS Clay Standards, NBS Spec. Publ. 260-37 (June 1972). COM72-50692**

Richard, J.C., and Hsia, J.J., Standard Reference Materials: Preparation and Calibration of Standards of Spectral Specular Reflectance, NBS Spec. Publ. 260-38 (May 1972). COM72-50528**

Clark, A.F., Denson, V.A., Hust, J.G., et al., Standard Reference Materials: The Eddy Current Decay Method for Resistivity Characterization of High-Purity Metals, NBS Spec. Publ. 260-39 (May 1972). COM72-50529**

McAdie, H.G., Garn, P.D., and Menis, O., Standard Reference Materials: Selection of Differential Thermal Analysis Temperature Standards Through a Cooperative Study (SRMs 758, 759, 760), NBS Spec. Publ. 260-40 (August 1972) COM72-50776**

Wood. L.A., and Shouse, P.J., Standard Reference Materials: Use of Standard Light-Sensitive Paper for Calibrating Carbon Arcs Used in Testing Textiles for Colorfastness to Light, NBS Spec. Publ. 260-41 (August 1972). COM72-50775**

Wagner, H.L., and Verdier, P.H., eds., Standard Reference Materials: The Characterization of Linear Polyethylene, SRM 1475, NBS Spec. Publ. 260-42 (September 1972). COM72-50944**

Yakowitz, H., Ruff, A.W., and Michaelis, R.E., Standard Reference Materials: Preparation and Homogeneity Characterization of an Austenitic Iron-Chromium-Nickel Alloy, NBS Spec. Publ. 260-43 (November 1972). COM73-50760**

Schooley, J.F., Soulen, R.J., Jr., and Evans, G.A., Jr., Standard Reference Materials: Preparation and Use of Superconductive Fixed Point Devices, SRM 767, NBS Spec. Publ. 260-44 (December 1972). COM73-50037**

Greifer, B., Maienthal, E.J., Rains, T.C., et al., Standard Reference Materials: Development of NBS SRM 1579 Powdered Lead-Based Paint, NBS Spec. Publ. 260-45 (March 1973). COM73-50226**

Hust, J.G., and Giarratano, P.J., Standard Reference Materials: Thermal Conductivity and Electrical Resistivity Standard Reference Materials: Austenitic Stainless Steel, SRMs 735 and 798, from 4 to 1200 K, NBS Spec. Publ. 260-46 (March 1975). COM75-10339**

Hust, J.G., Standard Reference Materials: Electrical Resistivity of Electrolytic Iron, SRM 797, and Austenitic Stainless Steel, SRM 798, from 5 to 280 K, NBS Spec. Publ. 260-47 (February 1974). COM74-50176**

Mangum, B.W., and Wise, J.A., Standard Reference Materials: Description and Use of Precision Thermometers for the Clinical Laboratory, SRM 933 and SRM 934, NBS Spec. Publ. 260-48 (May 1974). Superseded by NIST Spec. Publ. 260-113. COM74-50533**

Carpenter, B.S., and Reimer, G.M., Standard Reference Materials: Calibrated Glass Standards for Fission Track Use, NBS Spec. Publ. 260-49 (November 1974). COM74-51185**

Hust, J.G., and Giarratano, P.J., Standard Reference Materials: Thermal Conductivity and Electrical Resistivity Standard Reference Materials: Electrolytic Iron, SRMs 734 and 797 from 4 to 1000 K, NBS Spec. Publ. 260-50 (June 1975). COM75-10698**

Mavrodineanu, R., and Baldwin, J.R., Standard Reference Materials: Glass Filters As a SRM for Spectrophotometry-Selection, Preparation, Certification, and Use-SRM 930 NBS Spec. Publ. 260-51 (November 1975). COM75-10339**

Hust, J.G., and Giarratano, P.J., Standard Reference Materials: Thermal Conductivity and Electrical Resistivity SRMs 730 and 799, from 4 to 3000 K, NBS Spec. Publ. 260-52 (September 1975). COM75-11193**

Durst, R.A., Standard Reference Materials: Standardization of pH Measurements, NBS Spec. Publ. 260-53 (December 1978). Superseded by SP 260-53 Rev. 1988 Edition. PB88217427**

Burke, R.W., and Mavrodineanu, R., Standard Reference Materials: Certification and Use of Acidic Potassium Dichromate Solutions as an Ultraviolet Absorbance Standard, NBS Spec. Publ. 260-54 (August 1977). PB272168**

Ditmars, D.A., Cezairliyan, A., Ishihara, S., et al., Standard Reference Materials: Enthalpy and Heat Capacity; Molybdenum SRM 781, from 273 to 2800 K, NBS Spec. Publ. 260-55 (September 1977). PB272127**

Powell, R.L., Sparks, L.L., and Hust, J.G., Standard Reference Materials: Standard Thermocouple Material, Pt-67: SRM 1967, NBS Spec. Publ. 260-56 (February 1978). PB277172**

Cali, J.P., and Plebanski, T., Standard Reference Materials: Guide to United States Reference Materials, NBS Spec. Publ. 260-57 (February 1978). PB277173**

Barnes, J.D., and Martin, G.M., Standard Reference Materials: Polyester Film for Oxygen Gas Transmission Measurements SRM 1470, NBS Spec. Publ. 260-58 (June 1979). PB297098**

Chang, T., and Kahn, A.H., Standard Reference Materials: Electron Paramagnetic Resonance Intensity Standard: SRM 2601; Description and Use, NBS Spec. Publ. 260-59 (August 1978). PB292097**

Velapoldi, R.A., Paule, R.C., Schaffer, R., et al., Standard Reference Materials: A Reference Method for the Determination of Sodium in Serum, NBS Spec. Publ. 260-60 (August 1978). PB286944**

Verdier, P.H., and Wagner, H.L., Standard Reference Materials: The Characterization of Linear Polyethylene (SRMs 1482, 1483, 1484), NBS Spec. Publ. 260-61 (December 1978). PB289899**

Soulen, R.J., and Dove, R.B., Standard Reference Materials: Temperature Reference Standard for Use Below 0.5 K (SRM 768), NBS Spec. Publ. 260-62 (April 1979). PB294245**

Velapoldi, R.A., Paule, R.C., Schaffer, R., et al., Standard Reference Materials: A Reference Method for the Determination of Potassium in Serum, NBS Spec. Publ. 260-63 (May 1979). PB297207**

Velapoldi, R.A., and Mielenz, K.D., Standard Reference Materials: A Fluorescence SRM Quinine Sulfate Dihydrate (SRM 936), NBS Spec. Publ. 260-64 (January 1980). PB80132046**

Marinenko, R.B., Heinrich, K.F.J., and Ruegg, F.C., Standard Reference Materials: Micro-Homogeneity Studies of NBS SRM, NBS Research Materials, and Other Related Samples, NBS Spec. Publ. 260-65 (September 1979). PB300461**

Venable, W.H., Jr., and Eckerle, K.L., Standard Reference Materials: Didymium Glass Filters for Calibrating the Wavelength Scale of Spectrophotometers (SRMs 2009, 2010, 2013, 2014). NBS Spec. Publ. 260-66 (October 1979). PB80104961**

Velapoldi, R.A., Paule, R.C., Schaffer, R., et al., Standard Reference Materials: A Reference Method for the Determination of Chloride in Serum, NBS Spec. Publ. 260-67 (November 1979). PB80110117**

Mavrodineanu, R., and Baldwin, J.R., Standard Reference Materials: Metal-On-Quartz Filters as a SRM for Spectrophotometry SRM 2031, NBS Spec. Publ. 260-68 (April 1980). PB80197486**

Velapoldi, R.A., Paule, R.C., Schaffer, R., et al., Standard Reference Materials: A Reference Method for the Determination of Lithium in Serum, NBS Spec. Publ. 260-69 (July 1980). PB80209117**

Marinenko, R.B., Biancaniello, F., Boyer, P.A., et al., Standard Reference Materials: Preparation and Characterization of an Iron-Chromium-Nickel Alloy for Microanalysis: SRM 479a, NBS Spec. Publ. 260-70 (May 1981). SN003-003-02328-1*

Seward, R.W., and Mavrodineanu, R., Standard Reference Materials: Summary of the Clinical Laboratory Standards Issued by the National Bureau of Standards, NBS Spec. Publ. 260-71 (November 1981). PB82135161**

Reeder, D.J., Coxon, B., Enagonio, D., et al., Standard Reference Materials: SRM 900, Anti-epilepsy Drug Level Assay Standard, NBS Spec. Publ. 260-72 (June 1981). PB81220758

Interrante, C.G., and Hicho, G.E., Standard Reference Materials: A Standard Reference Material Containing Nominally Fifteen Percent Austenite (SRM 486), NBS Spec. Publ. 260-73 (January 1982). PB82215559**

Marinenko, R.B., Standard Reference Materials: Preparation and Characterization of K-411 and K-412 Mineral Glasses for Microanalysis: SRM 470, NBS Spec. Publ. 260-74 (April 1982). PB82221300**

Weidner, V.R., and Hsia, J.J., Standard Reference Materials: Preparation and Calibration of First Surface Aluminum Mirror Specular Reflectance Standards (SRM 2003a), NBS Spec. Publ. 260-75 (May 1982). PB82221367**

Hicho, G.E., and Eaton, E.E., Standard Reference Materials: A Standard Reference Material Containing Nominally Five Percent Austenite (SRM 485a), NBS Spec. Publ. 260-76 (August 1982). PB83115568**

Furukawa, G.T., Riddle, J.L., Bigge, W.G., et al., Standard Reference Materials: Application of Some Metal SRMs as Thermometric Fixed Points, NBS Spec. Publ. 260-77 (August 1982). PB83117325**

Hicho, G.E., and Eaton, E.E., Standard Reference Materials: Standard Reference Material Containing Nominally Thirty Percent Austenite (SRM 487), NBS Spec. Publ. 260-78 (September 1982). PB83115576**

Richmond, J.C., Hsia, J.J., Weidner, V.R., et al., Standard Reference Materials: Second Surface Mirror Standards of Specular Spectral Reflectance (SRMs 2023, 2024, 2025), NBS Spec. Publ. 260-79 (October 1982). PB84203447**

Schaffer, R., Mandel, J., Sun, T., et al., Standard Reference Materials: Evaluation by an ID/MS Method of the AACC Reference Method for Serum Glucose, NBS Spec. Publ. 260-80 (October 1982). PB84216894**

Burke, R.W., and Mavrodineanu, R., Standard Reference Materials: Accuracy in Analytical Spectrophotometry, NBS Spec. Publ. 260-81 (April 1983). PB83214536**

Weidner, V.R., Standard Reference Materials: White Opal Glass Diffuse Spectral Reflectance Standards for the Visible Spectrum (SRMs 2015 and 2016), NBS Spec. Publ. 260-82 (April 1983). PB83220723**

Bowers, G.N., Jr., Alvarez, R., Cali, J.P., et al., Standard Reference Materials: The Measurement of the Catalytic (Activity) Concentration of Seven Enzymes in NBS Human Serum (SRM 909), NBS Spec. Publ. 260-83 (June 1983). PB83239509**

Gills, T.E., Seward, R.W., Collins, R.J., et al., Standard Reference Materials: Sampling, Materials Handling, Processing, and Packaging of NBS Sulfur in Coal SRMs 2682, 2683, 2684, and 2685, NBS Spec. Publ. 260-84 (August 1983). PB84109552**

Swyt, D.A., Standard Reference Materials: A Look at Techniques for the Dimensional Calibration of Standard Microscopic Particles, NBS Spec. Publ. 260-85 (September 1983). PB84112648**

Hicho, G.E., and Eaton, E.E., Standard Reference Materials: A SRM Containing Two and One-Half Percent Austenite, SRM 488, NBS Spec. Publ. 260-86 (December 1983). PB84143296**

Mangum, B.W., Standard Reference Materials: SRM 1969: Rubidium Triple-Point - A Temperature Reference Standard Near 39.30° C, NBS Spec. Publ. 260-87 (December 1983). PB84149996**

Gladney, E.S., Burns, C.E., Perrin, D.R., et al., Standard Reference Materials: 1982 Compilation of Elemental Concentration Data for NBS Biological, Geological, and Environmental Standard Reference Materials, NBS Spec. Publ. 260-88 (March 1984). PB84218338**

Hust, J.G., Standard Reference Materials: A Fine-Grained, Isotropic Graphite for Use as NBS Thermophysical Property RMs from 5 to 2500 K, NBS Spec. Publ. 260-89 (September 1984). PB85112886**

Hust, J.G., and Lankford, A.B., Standard Reference Materials: Update of Thermal Conductivity and Electrical Resistivity of Electrolytic Iron, Tungsten, and Stainless Steel, NBS Spec. Pub 260-90 (September 1984). PB85115814**

Goodrich, L.F., Vecchia, D.F., Pittman, E.S., et al., Standard Reference Materials: Critical Current Measurements on an NbTi Superconducting Wire SRM, NBS Spec. Publ. 260-91 (September 1984). PB85118594**

Carpenter, B.S., Standard Reference Materials: Calibrated Glass Standards for Fission Track Use (Supplement to NBS Spec. Publ. 260-49), NBS Spec. Publ. 260-92 (September 1984). PB85113025**

Ehrstein, J.R., Standard Reference Materials: Preparation and Certification of SRM for Calibration of Spreading Resistance Probes, NBS Spec. Publ. 260-93 (January 1985). PB85177921**

Gills, T.E., Koch, W.F., Stolz, J.W., et al., Standard Reference Materials: Methods and Procedures Used at the National Bureau of Standards to Certify Sulfur in Coal SRMs for Sulfur Content, Calorific Value, Ash Content, NBS Spec. Publ. 260-94 (December 1984). PB85165900**

Mulholland, G.W., Hartman, A.W., Hembree, G.G., et al., Standard Reference Materials: Development of a 1mm Diameter Particle Size Standard, SRM 1690, NBS Spec. Publ. 260-95 (May 1985). PB95-232518/AS**

Carpenter, B.S., Gramlich, J.W., Greenberg, R.R., et al., Standard Reference Materials: Uranium-235 Isotopic Abundance Standard Reference Materials for Gamma Spectrometry Measurements, NBS Spec. Publ. 260-96 (September 1986). PB87108544**

Mavrodineanu, R., and Gills, T.E., Standard Reference Materials: Summary of the Coal, Ore, Mineral, Rock, and Refactory Standards Issued by the National Bureau of Standards, NBS Spec. Publ. 260-97 (September 1985). PB86110830**

Hust, J.G., Standard Reference Materials: Glass Fiberboard SRM for Thermal Resistance, NBS Spec. Publ. 260-98 (August 1985). SN003-003-02674-3*

Callanan, J.E., Sullivan, S.A., and Vecchia, D.F., Standard Reference Materials: Feasibility Study for the Development of Standards Using Differential Scanning Calorimetry, NBS Spec. Publ. 260-99 (August 1985). PB86106747**

Taylor, J.K., Trahey, N.M., ed., Standard Reference Materials: Handbook for SRM Users, NBS Spec. Publ. 260-100 (February 1993). PB93183796**

Mangum, B.W., Standard Reference Materials: SRM 1970, Succinonitrile Triple-Point Standard: A Temperature Reference Standard Near 58.08 C, NBS Spec. Publ. 260-101 (March 1986). PB86197100**

Weidner, V.R., Mavrodineanu, R., Mielenz, K.D., et al., Standard Reference Materials: Holmium Oxide Solution Wavelength Standard from 240 to 640 nm - SRM 2034, NBS Spec. Publ. 260-102 (July 1986). PB86245727**

Hust, J.G., Standard Reference Materials: Glass Fiberblanket SRM for Thermal Resistance, NBS Spec. Publ. 260-103 (September 1985). PB86109949**

Mavrodineanu, R., and Alvarez, R., Standard Reference Materials: Summary of the Biological and Botanical Standards Issued by the National Bureau of Standards, NBS Spec. Publ. 260-104 (November 1985). PB86155561**

Mavrodineanu, R., and Rasberry, S.D., Standard Reference Materials: Summary of the Environmental Research, Analysis, and Control Standards Issued by the National Bureau of Standards, NBS Spec. Publ. 260-105 (March 1986). PB86204005**

Koch, W.F., ed., Standard Reference Materials: Methods and Procedures Used at the National Bureau of Standards to Prepare, Analyze, and Certify SRM 2694, Simulated Rainwater, and Recommendations for Use, NBS Spec. Publ. 260-106 (July 1986). PB86247483**

Hartman, A.W., and McKenzie, R.L., Standard Reference Materials: SRM 1965, Microsphere Slide (10 μm Polystyrene Spheres), NIST Spec. Publ. 260-107 (November 1988). PB89153704**

Mavrodineanu, R., and Gills, T.E., Standard Reference Materials: Summary of Gas Cylinder and Permeation Tube Standard Reference Materials Issued by the National Bureau of Standards, NBS Spec. Publ. 260-108 (May 1987). PB87209953**

Candela, G.A., Chandler-Horowitz, D., Novotny, D.B., et al., Standard Reference Materials: Preparation and Certification of an Ellipsometrically Derived Thickness and Refractive Index Standard of a Silicon Dioxide Film (SRM 2530), NIST Spec. Publ. 260-109 (October 1988). PB89133573**

Kirby, R.K., and Kanare, H.M., Standard Reference Materials: Portland Cement Chemical Composition Standards (Blending, Packaging, and Testing), NBS Spec. Publ. 260-110 (February 1988). PB88193347**

Gladney, E.S., O'Malley, B.T., Roelandts, I., et al., Standard Reference Materials: Compilation of Elemental Concentration Data for NBS Clinical, Biological, Geological, and Environmental Standard Reference Materials, NBS Spec. Publ. 260-111 (November 1987). PB88156708**

Marinenko, R.B., Blackburn, D.H., and Bodkin, J.B., Standard Reference Materials: Glasses for Microanalysis: SRMs 1871-1875, NIST Spec. Publ. 260-112 (February 1990). PB90215807**

Mangum, B.W., and Wise, J.A., Standard Reference Materials: Description and Use of a Precision Thermometer for the Clinical Laboratory, SRM 934, NIST Spec. Publ. 260-113 (June 1990). PB90257643**

Vezzetti, C.F., Varner, R.N., and Potzick, J.E., Standard Reference Materials: Bright-Chromium Linewidth Standard, SRM 476, for Calibration of Optical Microscope Linewidth Measuring Systems, NIST Spec. Publ. 260-114 (January 1991). PB91167163**

Williamson, M.P., Willman, N.E., and Grubb, D.S., Standard Reference Materials: Calibration of NIST SRM 3201 for 0.5 in. (12.65 mm) Serial Serpentine Magnetic Tape Cartridge, NIST Spec. Publ. 260-115 (February 1991). PB91187542**

Mavrodineanu, R., Burke, R.W., Baldwin, J.R., et al., Standard Reference Materials: Glass Filters as a Standard Reference Material for Spectrophotometry-Selection, Preparation, Certification and Use of SRM 930 and SRM 1930, NIST Spec. Publ. 260-116 (March 1994). PB94-188844/AS**

Vezzetti, C.F., Varner, R.N., and Potzick, J.E., Standard Reference Materials: Anti-reflecting-Chromium Linewidth Standard, SRM 475, for Calibration of Optical Microscope Linewidth Measuring Systems, NIST Spec. Publ. 260-117 (January 1992). PB92-149798**

Williamson, M.P., Standard Reference Materials: Calibration of NIST Standard Reference Material 3202 for 18-Track, Parallel, and 36-Track, Parallel Serpentine, 12.65 mm (0.5 in), 1491 cpmm (37871 cpi), Magnetic Tape Cartridge, NIST Spec. Publ. 260-118 (July 1992). PB92-226281**

Vezzetti, C.F., Varner, R.N., and Potzick, Standard Reference Materials: Antireflecting-Chromium Linewidth Standard, SRM 473, for Calibration of Optical Microscope Linewidth Measuring System, NIST Spec. Publ. 260-119 (September 1992)

Caskey, G.W., Philips, S.D., Borchardt., et al., Standard Reference Materials: A Users' Guide to NIST SRM 2084: CMM Probe Performance Standard, NIST Spec. Publ. 260-120 (1994)

Rennex, B.G., Standard Reference Materials: Certification of a Standard Reference Material for the Determination of Interstitial Oxygen Concentration in Semiconductor Silicon by Infrared Spectrophotometry, NIST Spec. Publ. 260-121 (1994) PB95-125076/AS

Gupta, D., Wang, L., Hanssen, L.M., Hsai, J.J., and Datla, R.U., Polystyrene Films for Calibrating the Wavelength Scale of Infrared Spectrophotometer (SRM 1921). NIST Spec. Publ. 260-122 (1995) PB95-226866/AS

Development of Technology and the Manufacture of Spectrometric SRMs for Naval Brasses (MC62 M63). NIST Spec. Publ. 260-123 (IN PREP).

Strouse, G.F., SRM 1744: Aluminum Freezing Point Standard. NIST Spec. Publ. 260-124 (1995) SN003-003-03342-1

Schiller, S.B, Standard Reference Materials: Statistical Aspects of the Certification of Chemical Batch SRMs. NIST Spec. Publ. 260-125 (1996) PB96-210877/AS

Guenther, F.R., Dorko, W.D., Miller, W.R., et al., Standard Reference Materials: The NIST Traceable Reference Material Program for Gas Standards, NIST Spec. Publ. 260-126 (1996) PB96-210786/AS

Strouse, G.F., and Ahmet, A.T., Standard Reference Material 1747: Tin Freezing-Point Cell and Standard Reference Material 1748: Zinc Freezing-Point Cell. NIST Spec. Publ. 260-127 (IN PREP).

Zhang, Z.M., Gentile, T.R., Migdall, A.L., and Datla, R.U., Transmission Filters with Measured Optical Density at 1064 nm Wavelength--SRM 2036. SRM Spec. Publ. 260-128 (IN PREP).

*Send order with remittance to: Superintendent of Documents, U.S. Government Printing Office, Washington, DC 20102. Remittance from foreign countries should include an additional one fourth of the purchase price for postage.

**May be ordered from: National Technical Information Services (NTIS), Springfield, VA 22161.
For information phone (703-487-4650)
To Place an Order with PB# phone (800-553-6847)

Contents

Antireflecting-Chromium Linewidth Standard, SRM 473, for Calibration of Optical Microscope Linewidth Measuring Systems

J. E. Potzick
National Institute of Standards and Technology
Gaithersburg, Maryland 20899

ABSTRACT

This document describes the physical characteristics of Standard Reference Material SRM 473, provides instructions for its use in calibrating optical photomask linewidth measuring systems, and gives information and precautions concerning its care and handling.

Standard Reference Material SRM 473 was developed for use in calibrating optical microscopes for measuring linewidths in the range of 0.5 μm to 30 μm on antireflecting-chromium photomasks. In addition, it contains pitch (center-to-center) patterns ranging from 2 μm to 70 μm. The accurate measurement of feature dimensions on photomasks, such as those used in the production of integrated circuits, becomes increasingly difficult as the dimensions approach the wavelength of the light used to make the measurement. The effects of optical diffraction obscure the location of the feature edges. Raggedness and nonvertical walls along the edges add to the uncertainty of the measurement. This SRM makes possible traceable linewidth measurements by facilitating the evaluation of these and other components of linewidth measurement uncertainty.

The NIST linewidth measuring system and the procedures used to calibrate this SRM are discussed. These include the algorithm used for determining the line edge location from the optical intensity data, which incorporates a threshold criterion derived from analysis of microscope image profiles. The profiles are predicted by a numerical model based on the theory of partial coherence. The statistical performance of this system is monitored by measuring line features on a control photomask before and after calibrating each SRM. The factors that affect the calibration uncertainty are explained and evaluated.

NIST photomask linewidth SRMs 473, 475, and 476 are available from the Office of Standard Reference Materials, NIST, EM 205, Gaithersburg, Md. 20899. Voice 301-975-6776, FAX 301-948-3730.

KEY WORDS: accuracy; antireflecting-chromium; calibration; control charts; critical dimensions; integrated circuits; linewidth measurement; optical microscope; photomask; pitch, semiconductor industry; standard reference material; statistical process control; threshold; measurement uncertainty.

1. Introduction

The ability to measure and control critical dimensions during the production of integrated circuits is essential to the semiconductor industry. Many measuring systems claiming high precision are now commercially available for use in determining some of these critical dimensions. The only way the accuracy of a measurement can be assessed is through its traceability to a recognized standard. As part of a continuing effort to provide means for calibrating these systems, the National Institute of Standards and Technology (NIST) has developed Optical Microscope Linewidth Measurement Standard Reference Materials

Standard Reference Material (SRM) 473 is designed for calibrating optical microscope systems to measure linewidths on antireflecting-chromium photomasks.* It was produced with conventional technology by a commercial photomask manufacturing facility. In addition to isolated opaque and clear lines for linewidth calibration, this SRM contains line patterns for checking length scale, adjusting video-type micrometers, and detecting mechanical or optical nonlinearities. The design of the calibrated pattern is described in section 2.

Section 3 gives information and precautions on the care and use of this SRM to calibrate an optical linewidth measuring system. Because of the variety of linewidth measuring systems in use today, no attempt has been made to give specific instructions for each type of microscope.

To calibrate the SRM line features, a photometric microscope with lenses selected for least aberration was modified at NIST. Except for the initial positioning, aligning, and focusing of the photomask, the entire calibration process is automated. The line features are illuminated in transmission with partially coherent green light (wavelength 0.53 μm) from a filtered incandescent source. The linewidths are determined from the image profile (*image intensity* versus *position* across a feature). A considerable amount of theoretical work was conducted to establish the location on the observed image profile that corresponds to the physical edge of a feature [2]. The quality of the feature edge geometry of samples near the beginning and end of each production batch of SRM photomasks is examined with a scanning electron microscope (SEM). The calibration uncertainty given in the certificate is based on this sampled edge geometry and the agreement between theoretically modeled and experimentally generated image profiles. Section 4 contains brief descriptions of the NIST linewidth calibration system and the automated calibration process as well as discussions of the line edge location algorithm. Calibration uncertainty is discussed in section 5. The process control procedures used in the calibration of this SRM are discussed in some detail in the Appendix.

*Binary and phase shift photomasks can also be measured accurately by emulating the stepper aerial image. See Reference [1].

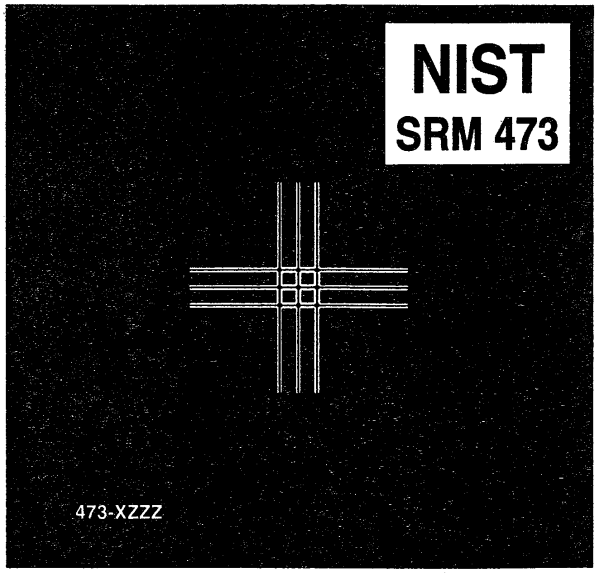

FIGURE 1. A view of the overall pattern on SRM 473. The basic measurement pattern is repeated eight times about the center. The horizontal and vertical lines help locate the patterns. The overall form is that of a standard 5-inch photomask.

2. Physical Characteristics of SRM 473

SRM 473 is made from an antireflecting-chromium photoplate by conventional photolithographic techniques. The substrate is a quartz plate of a type commonly used for fabricating integrated circuit photomasks, nominally 127 mm × 127 mm × 2.3 mm (5.0 in. × 5.0 in. × 0.09 in.). The nominal thickness of the chromium layer is 100 nm. These photomasks are not equipped with pellicles.

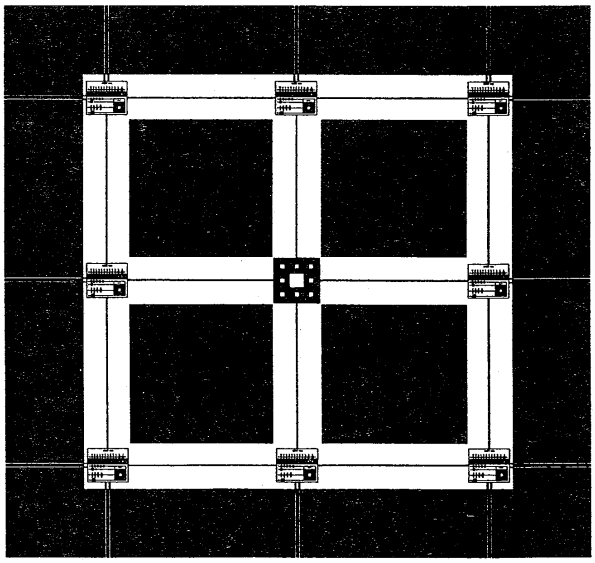

FIGURE 2. An enlarged view of the center of the SRM. The pattern number given with the serial number on the certificate identifies which basic pattern has been calibrated by NIST. Pattern No. 1 is in the upper left; pattern No. 8 is in the lower right. Pattern identification numbers are included within each basic pattern as shown in figure 3. This array of eight patterns occupies an area of approximately 9 mm × 9 mm.

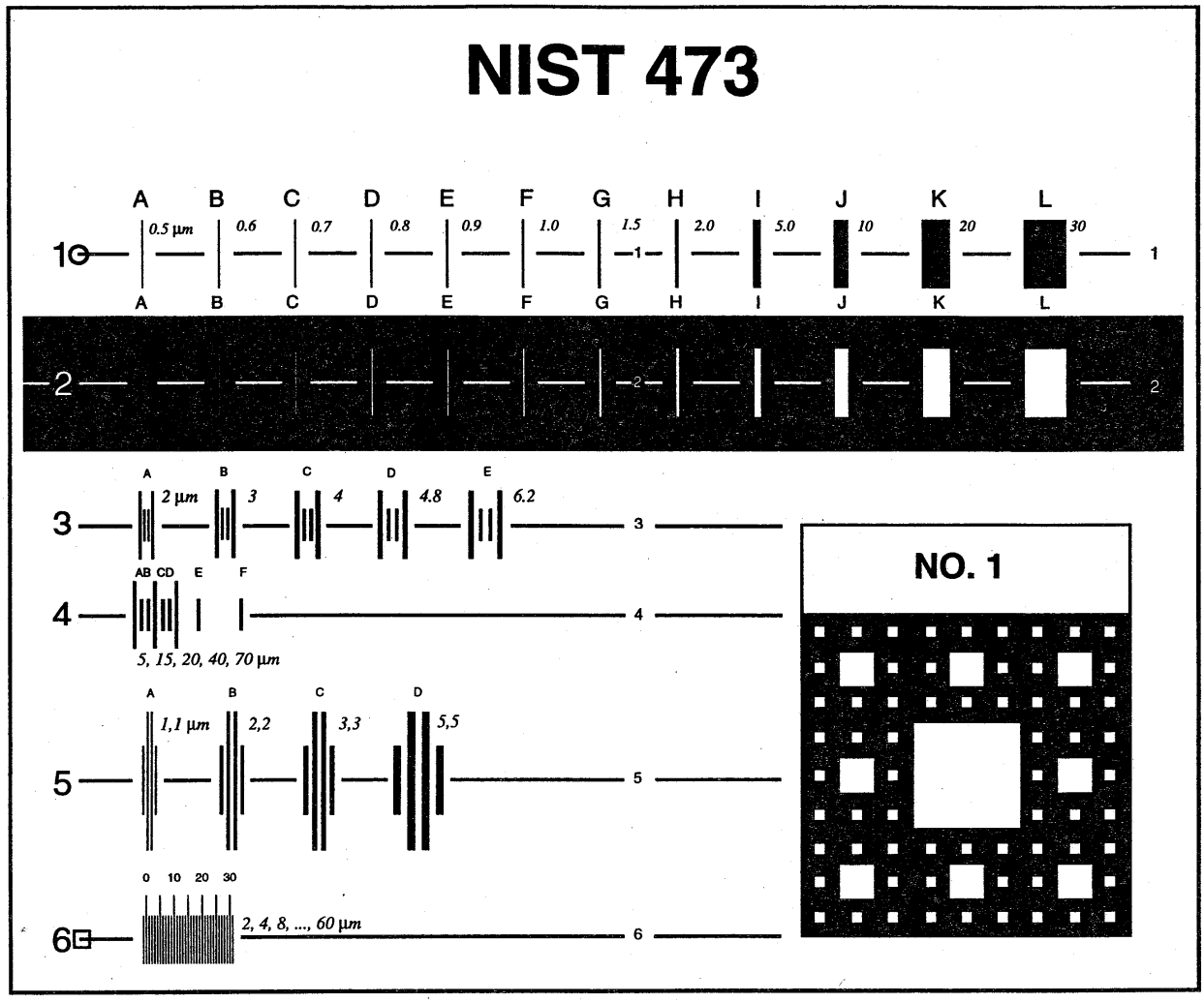

FIGURE 3. A view of one basic measurement pattern on the SRM. The individual features are located by reference to an alphanumeric code with numbers identifying the row and letters designating the position within the row. The broken horizontal lines mark the central calibrated area of the features. The box surrounding the overall pattern is used to align the pattern on the measurement system. The size of this box is 873 µm × 724 µm. The pattern identification number can be seen in the box above the carpet design in the lower right.

Calibration values are given for: widths of opaque lines in row 1 and clear lines in row 2; center-to-center spacing of the two inner (short) lines of each feature in row 3; center-to-center spacing from line A to lines B through F in row 4; widths of the left inner (long) line and the space to its right of each feature in row 5; and center-to-center spacings from line 0 to lines one through 30 in row 6. The nominal width and pitch values in µm are written on this figure in *italics*; they are not printed on the photomask.

Figure 1 shows the overall pattern on the chromium-coated side of the standard. The three horizontal and three vertical intersecting lines help locate the basic measurement pattern which is repeated at eight locations around the center of the standard as shown in figure 2 (a magnified view of the central area of figure 1). A pattern identification number (1 through 8) is located within each basic pattern. Only one of these eight patterns is chosen after visual inspection to be certified. The certificate accompanying the SRM gives the number of the certified pattern. The carpet design at the center of the photomask as well as those within each basic pattern are focusing aids and contain no calibrated features.

Figure 3 shows the details of the features in each of the eight identical patterns on the SRM. The pattern identification number can be seen in the lower right quadrant, just above the carpet design. The vertical sides of the box surrounding the basic pattern are parallel to the calibrated line features and may be used to aid in aligning the SRM features to be perpendicular to the measurement axis.

The calibrated features are arranged in six rows. Row numbers are located at the ends of each row. Each feature within rows 1 through 5 is further identified by a letter, A through L, located immediately above the feature. Thus, 1E refers to the opaque line in row 1 at position E. Row 6 contains a single multiple-line feature with every 5th line elongated and every 10th line numbered. All rows on the SRM contain a broken horizontal fiducial line which de-

fines the measurement position on each feature.

Row 1 consists of 12 opaque lines (1A through 1L) on a clear background, and row 2 consists of 12 clear lines (2A through 2L) on an opaque background. These opaque and clear lines are used for calibrating optical microscopes used to measure linewidths of isolated lines of either or both polarities. Nominal linewidths of these features range from 0.5 μm to 30 μm.

Rows 3 and 4 are intended to be used for calibrating optical microscopes for making line spacing (pitch) measurements as well as for making initial length scale adjustments when calibrating linewidth measurement systems. Row 3 consists of five features (3A through 3E), each with four opaque lines. Certified values are given for the pitch of the two interior (short) lines** of each feature. Nominal pitches for these features range from 2.0 μm to 6.2 μm. Row 4 contains a series of nine opaque lines, with certified pitch values given for the six short lines (4A through 4F) only. The values given on the certificate are for the pitches from line 4A to lines 4B through 4F. Pitches for the other combinations of lines (*e.g.*, 4B to 4E) can be calculated from the certificate values, giving an array of nominal pitch values from 5.0 μm to 70 μm.

Row 5 consists of four multiple-line features (5A through 5D) with approximately equal line and space widths. The widths of the left interior line and central space are certified. Nominal widths range from 1.0 μm to 5.0 μm. These features are useful for adjusting brightness and contrast of video image-scanning instruments and setting variable-threshold systems to achieve the proper line-to-space ratio.

The calibrated feature in row 6 is a series of 33 opaque lines, nominally 1.0 μm wide with 2.0 μm center-to-center spacing; distances from line 0 to lines 1 through 31*** are certified. This feature is intended to be used as a linear scale in checking for mechanical nonlinearities and optical distortions in the linewidth measurement system (*e.g.*, the magnification as a function of position over the field of view) and for checking the resolving power of the microscope objective.

3. Using SRM 473

The following section provides information on the care and handling of the SRM photomask and gives basic instructions and precautions on its use for calibrating optical microscope systems for measuring linewidths of features on antireflecting photomasks or similar artifacts.

3.1 Special precautions The certification for NIST photomask linewidth standards SRM 473 will remain valid as long as the calibrated patterns remain undamaged. The materials used are stable and there is no reason for the dimensions to change significantly relative to the stated calibration uncertainty. It is important that these standards be handled with care, be free of scratches and dirt, and be cleaned properly when necessary. Abrasion and chemical corrosion must be avoided.

Contamination or damage can change the measured linewidths, invalidating the NIST calibration. Particular care should be taken during use to avoid bringing the microscope objective, or any other object, into contact with the top (chromium-coated) surface of the SRM. It is recommended that users calibrate secondary standards of their own design and use these in routine calibrations while keeping the NIST standard in safe storage. If this is done, the secondary standards should be checked periodically against the NIST standard. Also, it may be advisable for the user to calibrate one or more of the uncalibrated patterns on this SRM for use in the event that the NIST calibrated pattern is destroyed.

Recertification A recertification service is not available for these standards because the artifact stability renders this unnecessary and the cost would be comparable to that for a new standard. If there is any reason to question the provenance of one of these standards, it must be replaced with a new one.

Cleaning Precautions should be taken to prevent the accumulation of airborne and other contaminants on the SRM. If cleaning becomes necessary, use only noncorrosive wetting solutions (surfactants) at room temperature.

For cleaning we recommend the following procedure:

- Soak the SRM for 15 minutes to several hours in a mild solution of commercial mask cleaner and deionized water.
- While the mask is still immersed, brush the coated side gently with a soft lens brush; stroke parallel to the calibrated line length and in one direction.
- Rinse the mask thoroughly with deionized water.
- Blow away water droplets with a stream of clean dry air or nitrogen at room temperature.

If the contamination persists, apply a few drops of undiluted mask cleaner directly on the SRM before repeating the above cleaning process.

Removing fingerprints or other greasy contamination may require rinsing the SRM with alcohol or acetone and repeating the above cleaning process.

3.2 Metrology issues Inappropriate use of the NIST linewidth standards can result in inaccurate calibrations and may invalidate traceability to NIST. The practices most apt to give inaccurate calibrations when using the NIST linewidth standard include:

**The two outer lines of each pattern in row 3 and the three unlettered (long) lines in row 4 serve as "guard lines" during the photolithographic etching process to equalize proximity effects along the line edges and are not calibrated.

***The two outer lines of each pattern in rows 5 and 6 serve as "guard lines" during the photolithographic etching process to equalize proximity effects along the line edges and are not calibrated.

a. ***Using the linewidth standard to calibrate a measurement system that will then be used to measure linewidths on specimens with optical properties that differ significantly from those of the standard (for example, features on silicon wafers).*** One important requirement for accuracy is that the image profile (or diffraction pattern) of the edge have the same shape for both the standard and the user's specimens. These image profiles will not have the same shape if the optical properties of the standard and the user's specimens differ.

When calibrating optical measuring systems that use transmitted light, it is especially important that the transmittance of the chromium film on the standard and the user's specimen match at the measuring wavelength. The transmittance of SRM 473 is less than 0.2% at a wavelength of 0.53 μm. Line edge location conditions for photomasks with transmittance greater than about 0.5% may be significantly different from those of this SRM.

When calibrating optical measuring systems that use reflected light, the standard and the user's specimen must match even more closely, and this measurement configuration is strongly discouraged. The more important properties to match are the complex reflection coefficient of the patterned metal layer and the substrate, the thickness of the patterned layer, and the transmittance of the patterned layer. Measurement of linewidths in reflected light is not recommended because of the difficulty in measuring and matching these parameters.

b. ***Using the linewidth standard to calibrate a scanning electron microscope.*** This SRM is designed specifically for use with optical microscopes and, without extensive modeling of the electron-specimen-instrument interactions, this SRM cannot be used to calibrate an SEM for linewidth measurements. Its use in an SEM is further discouraged because the profile of the feature could change as a result of coating the SRM with an evaporated film to reduce electrical charging, of deposition of contamination during operation of the SEM, and of detachment of the chromium during cleaning to remove evaporated films or contaminants. (The substrate of this SRM is quartz and, even when low-voltage SEM techniques are used it is next to impossible to view the SRM features in the SEM without first coating the sample.)

c. ***Failing to correct for scattered (or flare) light.*** Although the chromium pattern on SRM 473 is not highly reflective, it includes isolated features surrounded by various large clear areas and the image profiles may exhibit a moderate component of scattered light which may vary from feature to feature and from the user's specimen. The intensity of the scattered light should be subtracted from all measured intensity levels before determining the edge location (section 4.4). This correction has been made in the calibration of SRM 473.

At the present time, NIST has two other linewidth standards (SRMs 475 and 476), both in the form of a standard 2.5 inch photomask. These two SRMs have a more limited range of linewidths than SRM 473. SRM 476 is patterned with bright chromium and SRM 475 is patterned, as is SRM 473, with antireflecting chromium. We recommend that the user: (1) use the SRM that most closely matches the specimens to be measured and (2) make the scattered light correction outlined above.

d. ***Using the NIST linewidth standards to generate a calibration curve that is then used for features that are larger than the largest or smaller than the smallest feature on the standard.*** The nominal linewidth range of SRM 473 is from 0.5 μm to 30 μm and this SRM will not adequately calibrate a microscope outside of this range. This is especially true for extensions much below the nominal range where the calibration curve may become nonlinear due to proximity or other effects (see below).

A photomask with substrate thickness different from that of the standard can be measured without incurring added uncertainty. It may be necessary to refocus the condenser lens for differing substrate thicknesses.

The user should be aware that all standards have an uncertainty of calibration associated with them and, to this extent, are not perfect. The calibration of a microscope using a standard has an imprecision associated with that calibration and also has an imprecision associated with the subsequent use of that calibrated microscope to measure an unknown specimen. Therefore, the accuracy of the user's measurements cannot exceed the accuracy of the standard. The uncertainty of the final measurement on the unknown specimen is a combination of the accuracy of the standard used for calibration, the precision of the calibration measurements using the standard, and the precision of the measurements of the unknown specimen.

These and other topics are discussed more fully in the references and bibliography. The need to use good measurement techniques to achieve the best results with these linewidth standards cannot be overemphasized. The user who knows more about the potential problems is more likely to make better use of the linewidth standard.

3.3 Proximity effects A measuring instrument which scans the object to form an image has a finite size resolution element, defined in this context as the total specimen volume which contributes significantly to the image at any point in the scan. Note this is different from the imaging resolution or measurement resolution. The apparent position of an object (a line edge, for example) can be influenced by the proximity of another object within this resolution element, causing an error when measuring its position.

In an SEM the diameter of the incident electron beam may be less than one nanometer, but it can penetrate and interact with the specimen in a volume perhaps several tenths of a micrometer wide or more depending on the instrument's

operating conditions. If the collected electrons or their progenitors originate within this volume, then the resolution element is this interaction volume and is much larger than the beam diameter. Multiple electron scattering from surface topography of nearby objects can also contribute to the size of the resolution element. The optical equivalent is the Airy disk of the microscope, which is on the order of the wavelength of the illumination ($1.22\lambda/NA$), again several tenths of a micrometer. The scanning probe equivalent is the effective radius of the probe tip (including probe-to-specimen interaction distance) combined with possible subsurface interactions, cantilever bending, and possible migration of the effective probe contact point on the tip due to object topography. Most of these SPM issues, however, will not lead to proximity effects.

The consequence of this proximity effect is a possible error when measuring the width of a narrow line or the pitch of lines near the end of a dense line/space array. The effect can lead to nonlinearity in linewidth measurement when both line edges are within the resolution element. If the pitch of a line array is smaller than the resolution element the microscope sees different objects at the end of the array and at the interior because of the loss of translational symmetry near the end. The pitch measurement can then incur an error near the ends of a dense array that is absent for the interior lines, while no such error occurs anywhere along an array with larger pitch.

There can be similar proximity effects during fabrication, for example in exposure and etching, and these must be distinguished from measurement proximity effects. The common way to avoid proximity effects in pitch measurement is to add guard lines at the ends of the array; these lines are patterned and printed the same as the other lines but they are not measured. The features in rows 3 to 6 all contain guard lines.

3.4 Microscope calibration procedures The following procedures are recommended for using this SRM to calibrate optical microscope systems for measuring linewidths on antireflecting photomasks. It is assumed the user is familiar with the operation of the microscope system being calibrated; no attempt is made to give detailed instruction on the use of microscope systems. The steps marked with an asterisk(*) need only be performed the first time the system is used or after any changes have been made in the measurement system.

MICROSCOPE CALIBRATION PROCEDURE

PROCEDURE	EXPLANATORY NOTES
1. Set up the measurement system for dimensional measurements; use the same procedures that will be used or measuring photomasks.	Follow manufacturers instructions or consult reference [3] for recommended procedures including adjustments for Köhler illumination.
2. Locate the specific basic pattern on the SRM that has been calibrated by NIST within the microscope field-of-view.	The pattern identification number is located in the box above the carpet design in the lower right (see fig. 3). The identification number of the calibrated pattern is given on the SRM certificate.
3.* Check the resolving power of the microscope objective by focusing on row 6.	If the objective cannot resolve clearly the lines in this feature, use another objective.
4. Align the SRM so that lines are measured in a direction perpendicular to their length.	The box surrounding the basic pattern group (see fig. 3) may be used as an alignment aid to minimize cosine errors.
5. Adjust the measurement system length scale to give the same reading as the NIST value for the spacing of appropriate line pair(s) in row(s) 3 or 4.	The line pair(s) chosen should have spacing in the same range as the dimensions of the features to be measured by the user.
6.* Check for mechanical nonlinearity and/or optical distortion by measuring the spacings of the lines in row 6, and compare the results with the NIST values.	For all further measurements, use only the portion of the field of view corresponding to the location where the differences from NIST values are relatively constant or that portion of the video display which exhibits minimum distortion.
7. Adjust system contrast, brightness (on video-type image-scanning systems) and/or threshold level until the measured widths of both the line and space of an appropriate feature in row 5 agree as closely as possible with the NIST values. Use these same settings throughout this measurement session.	The feature chosen should have widths within the range of the anticipated measurements. Compensate for flare light during this process and for all subsequent measurements (see paragraph *c.*, sec. 3.2).

NOTE: If any changes other than refocusing, repositioning, and adjusting for flare are inadvertently made during the following steps, discard the data and start again with step 5.

8.	Measure and record the widths of the calibrated features in rows 1 and 2 and/or the pitches in rows 3 and 4.	Use the same focusing criteria throughout and make all measurements in the same direction of travel. Compensate for flare light on all photomasks (not only this standard).
9.	Derive the calibration curves as described in reference [4].	These calibration curves apply only to this system/operator

After performing these procedures, the system is now ready for measurement of other antireflecting-chromium photomasks or artifacts with optical properties similar to SRM 473 (low reflectance and very low transmittance) using the same threshold value and flare-light correction procedure. If the user attempts to measure artifacts with chromium layers having transmission much greater than 0.2%, it may be necessary to measure the phase angle, ϕ, and use eq (3) (section 4.5) to determine a different edge location threshold. These procedures are beyond the scope of this report.

Repeat the complete calibration procedure on a routine periodic basis and whenever a substantial change is made in the measurement system. The time between periodic calibrations may have to be determined empirically.

4. Calibration of SRM 473

All measurements at NIST of the SRM feature dimensions were performed on the automated optical linewidth system [5] in a laboratory with temperature controlled at 21 ± 2 °C. Linewidths and pitches are determined from the optical profile data. The uncertainty of the calibrations is a combination of the uncertainties of the measurement process, of the feature edge location algorithm, and of the geometry of the physical edge of the measured features. Data acquisition and processing are entirely automated, and the data are untouched by human hands (no manual data transfers, no editing allowed; except for scale factor entry, see below) from acquisition through certificate printing and archival storage.

4.1 The measurement system The measurement system, diagrammed in figure 4, is built around a carefully aligned optical transmission microscope mounted on a vibration isolation table. The photomask is placed on a scanning piezoelectric flexure-pivot stage with finely controlled motion in the x (scanning) and z (focus) directions; this stage is mounted on another stage with coarse motion leadscrews in the x and y directions to allow positioning of the desired feature in the field of view.

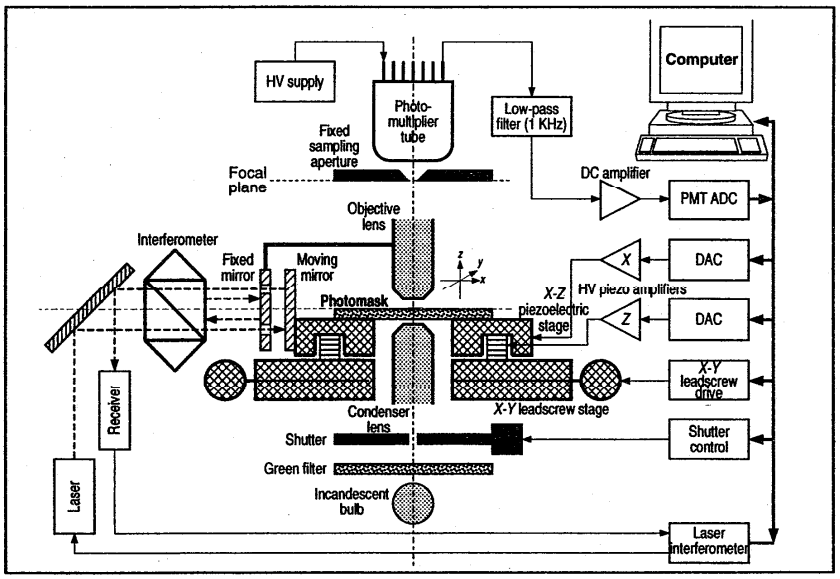

FIGURE 4. Schematic of the NIST automated optical linewidth calibration system. The photomask is placed on the scanning piezoelectric stage and is illuminated from below with partially coherent light from a filtered incandescent source. The sampling aperture remains fixed while the magnified image of the feature being measured is scanned past the slit by moving the photomask. The motion is measured with a laser interferometer and the image intensity at the slit is monitored with a photomultiplier tube. The amplified and digitized output of the photomultiplier and the interferometer output are connected via the IEEE-488 bus to the computer.

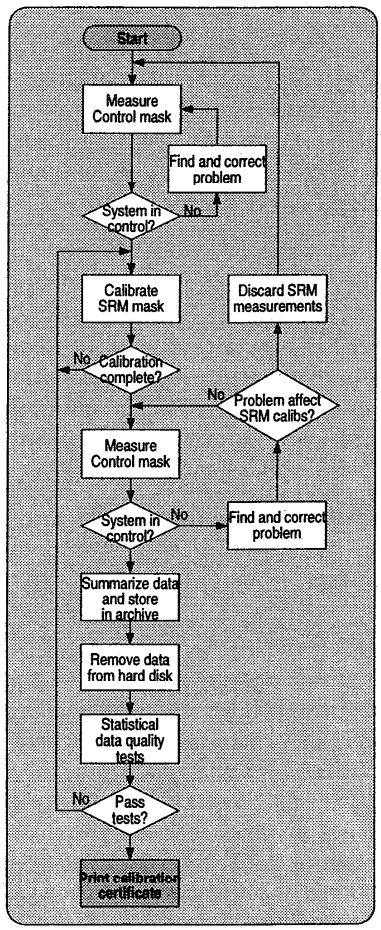

FIGURE 5. Flow chart outline of the overall calibration procedure for SRM photomasks with the NIST optical linewidth measurement system. First, measurements are made on a control photomask and tested statistically to determine if the system is operating properly. Then, the SRM photomask is calibrated and the system operation is checked again by measuring the control photomask. A calibration certificate can be printed for the SRM photomask only if all tests indicate the system is within statistical control.

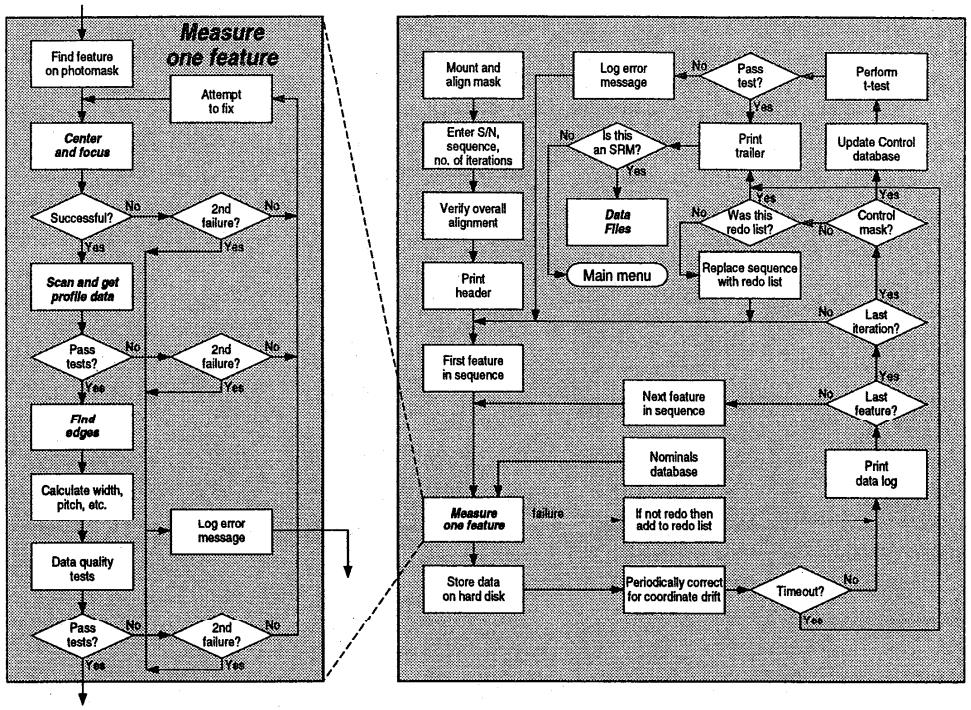

FIGURE 6. Flow chart of the main steps of the measurement sequence performed by the NIST optical linewidth measurement system. Each feature on the SRM photomask is centered in the microscope field of view, focused, and measured in sequence. The sequence is repeated until each feature has been measured nine times. The optical profile position (X) and intensity (P) are measured and treated as two one-dimensional arrays. Then the edge threshold level and corresponding edge positions are derived from these data.

The specimen is measured in visible transmitted light by scanning the stage at constant velocity, and simultaneously measuring the intensity of the magnified image through a sampling aperture fixed on axis in the image plane, and the position of the scanning stage with a laser interferometer. Scanning the specimen stage is preferable to scanning the slit (or using a CCD scan) as it provides a more direct link to the SI unit of length. Measurement accuracy is more important here than measurement speed. The photomask is illuminated from below with Köhler illumination (*i.e.*, each point on the lamp filament evenly illuminates the entire specimen) from an incandescent source filtered at 530 nm wavelength (~60 nm bandwidth) with a coherence parameter of 2/3 (0.6 numerical aperture condenser lens and 0.9 numerical aperture objective lens). A 20 μm × 400 μm slit is fixed on axis in the image plane in front of a photomultiplier tube. Image magnification at the slit is 157 times, giving an effective measurement area on the photomask of 0.127 μm × 2.55 μm, which is centered top-to-bottom on the feature (at the fiducial line). The photomultiplier output is amplified and digitized by a 16-bit analog-to-digital converter (ADC). Stage motion in the scanning direction is measured by a differential laser interferometer with resolution of 125 points per micrometer. All these devices are connected via appropriate control hardware and IEEE-488 bus to a dedicated desktop digital computer.

4.2 SRM Calibration Procedure An outline of the overall calibration procedure is charted in figure 5. Before each complete SRM calibration, selected features on a Control photomask are measured and compared with Control history to ensure that the system has not changed or drifted. These selected features include spacing patterns 3E, 4F, and row 6 which have been independently calibrated on the NIST Linescale Interferometer [6] to provide traceability to the standard meter. Each feature on the SRM being calibrated is then measured in sequence and the sequence repeated nine times. Every feature is calibrated, and this process takes about seven hours. After each SRM calibration is completed, the Control photomask is measured again.

All measurements, including the Control measurements, are entered into the linewidth database. After the calibration measurements are completed the database is searched to ensure that the Control was measured before and after the calibration and that these two Control measurements were statistically invariate. The database entries for the calibration are combined and examined statistically: the standard deviation for each feature is calculated, possible outliers identified, number of measurements checked, time interval between Control measurements and calibration measurements checked, etc. Criteria must be met for each of these statistical factors. If necessary, more measurements can be made and added to the database.

Once all the above conditions are met, the certificate is printed and the SRM linewidth standard is released to the Standard Reference Materials Program Office for sale. All of the calibration database files for this serial number are then stored on one flexible disk along with summary data. The disk is kept for archival storage along with the printed calibration results for each measurement, a printed summary of the statistical data, and dark-field illumination micrographs of the calibrated pattern.

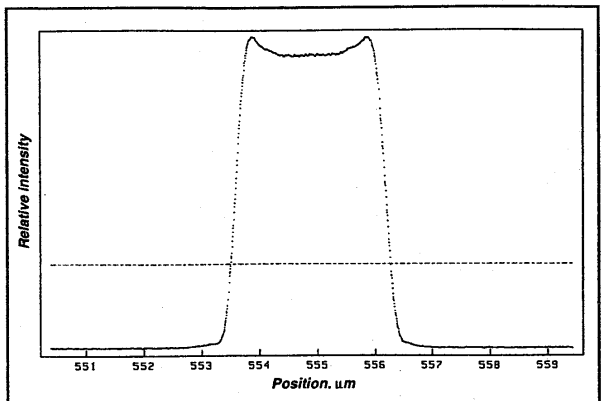

A. Profile typical of a clear line (space) in row 2.

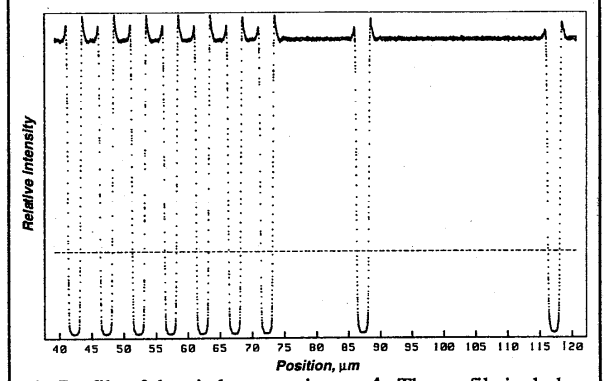

B. Profile of the pitch pattern in row 4. The profile includes guard lines as well as the line-spacing pairs.

FIGURE 7. Samples of optical profiles (measured *light intensity* vs *position*) displayed on the computer screen during the calibration process. The vertical axes are relative light intensity and the horizontal axes are position in micrometers. Each dot is a data point. The horizontal lines mark the edge threshold.

4.3 Feature measurement sequence A flow chart of the main steps of the feature measurement sequence is given in figure 6. The calibration computer first centers the feature to be measured in the field of view, focuses, and then scans while acquiring the optical profile position and intensity data and then storing them as two one-dimensional arrays. At the beginning and end of each scan the shutter is closed in order to measure the photometer dark offset. The scan data are then corrected for offset and offset drift. The data are then low-pass filtered to reduce extraneous noise and processed to find the edge locations. Linewidth or pitch is then calculated.

Position and intensity data points are correlated during the scan by alternately triggering the interferometer and the a-d converter to take one reading each in a software loop while the scanning stage is moving. There may be a few CPU clock cycles delay δt between the two readings of a data pair, but this delay is very small and is the same at leading and trailing edges of a line; thus, it cancels in both linewidth and pitch calculation. The effect is to slide the x axis by an amount $\delta t \times$ *scan velocity*, but both leading and

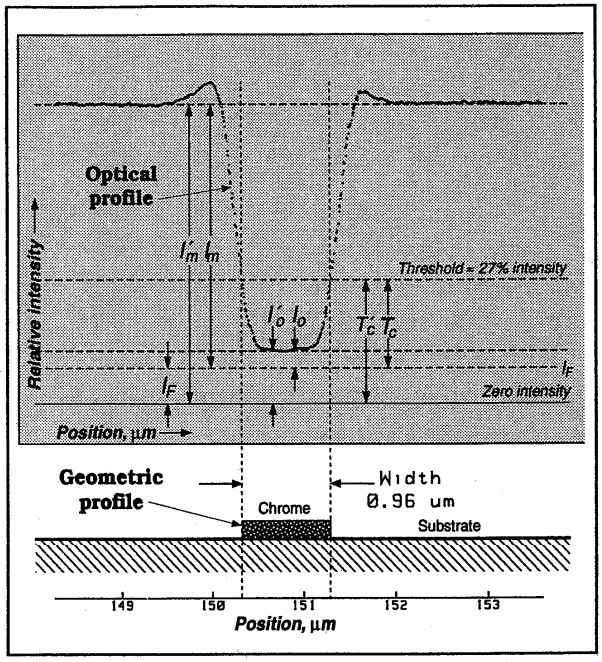

FIGURE 8. Schematic of the cross section of a vertical-edged chromium line and the corresponding optical profile of its microscope image. I_m is the intensity of the light passing through the clear area; I_o is the intensity of the light passing through the chromium; T_c is the intensity at the physical edge (threshold); I_f is the intensity of the flare light. The prime designates an observed intensity. The vertical axis is optical intensity and the horizontal axis is position.

trailing edges slide by the same amount if the velocity is constant, and no measurement error ensues.

If vibration or trigger jitter are present this delay contributes to the variance of the data because the scan velocity at the leading edge may not be the same as at the trailing edge. For the typical scan velocity of 2 µm/sec, if the scan velocity changes by 100% at one edge, the effect is 2 nm per ms of delay.

Image profiles such as those in figure 7 are presented on the computer screen during data acquisition and processing to allow monitoring system operation. After passing several data quality checks, the results are entered into a database for the SRM being calibrated.

A more detailed description of the measurement sequence and system can be found in reference [5].

4.4 Edge location determination Analysis of optical microscope imaging gives the following equation for image intensity at the edge of a line [7]:

$$T_c = R_t(I_o + I_m + 2(\sqrt{I_o I_m})\cos\phi) \qquad (1)$$

where T_c is the intensity of the light at the threshold point (edge) on the image profile (see figure 8); I_o is the intensity of the light passing through the not-perfectly-opaque chromium layer; I_m is the intensity of the light passing through the clear areas (beyond the diffraction peaks); and ϕ is the optical phase difference of the light transmitted through these two areas. R_t is a theoretically derived ratio, of ap-

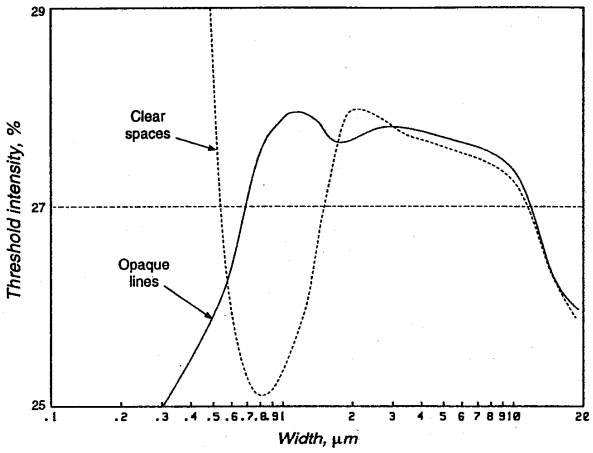

FIGURE 9. Optical intensity [% of (I_m-I_o)] at edge location versus linewidth, from a computer model of the NIST calibration system. Transmittance of the chrome equals 0.2% and ϕ equals $\pi/2$ radians.

proximately 0.25, which varies slightly depending on the coherence factor, viewing slit width, focus, proximity of the next edge, and other imaging conditions. For the conditions of measurement of this SRM in the NIST calibration system, R_t varies from 0.25 to 0.28 (see last paragraph of this section).

Real microscope images often include some flare light (light scattered off the microscope components illuminating the otherwise opaque features on the photomask from above or reaching the image plane by indirect paths). In nonlaser illumination systems, this light is temporally incoherent with respect to the light comprising the diffraction pattern (image profile) and simply adds incoherently (intensity-wise) to each intensity of the image profile.

To a first approximation the intensity of the flare light is not a function of position across a feature. Therefore, the effect of the flare light can be incorporated into eq (1) by simply subtracting its value from each intensity component on the image profile:

$$I_o = I_o' - I_f,\ I_m = I_m' - I_f,\ T_c = T_c' - I_f, \qquad (2)$$

where the prime designates an observed intensity (including the effects of diffraction, transmission, and flare) and where I_f is the magnitude of the flare light component in the image profile for each feature. Substituting into eq (1) gives:

$$T_c' = R_t[(I_o' - I_f) + (I_m' - I_f) + 2\sqrt{(I_o' - I_f)(I_m' - I_f)}\ \cos\phi] + I_f \qquad (3)$$

Both ϕ and I_f must be known to evaluate the threshold condition. I_f is feature and background dependent and must be determined for each feature. For this SRM, where the antireflecting-chromium layer can be considered to be homogeneous, the transmittance T_r and ϕ can be taken as constants and I_o can be expressed as $(T_r \times I_m)$. Then, considering that $(I_m - I_o)$ equals $(I_m' - I_o')$ and substituting in eq (2), it can be shown that

$$I_f = [I_o' - (T_r \times I_m')]/(1 - T_r) \qquad (4)$$

The transmittance of the SRM was determined by using the linewidth measuring system to measure the intensity of light passing through the chromium near the center of the large chromium-covered upper-left quadrant of the mask, and found to be about 0.17% of the incident intensity.

For the SRM user, determination of I_f for each feature by using eq (4) would be time consuming and impractical; however, when, as for this SRM, the transmittance is low (less than 0.2%), I_0' and I_f are nearly identical and the user may consider all measured I_0' intensity to be flare light. Then the correction for flare light can be implemented simply by one of the following actions: shift the intensity zero level so that $I_0'=0$; subtract I_0' from the measured intensities; determine the threshold level as a percent of $(I_m'- I_0')$. If the user cannot make this correction, the reflectance and transmittance of the standard used for calibration should match the reflectance and transmittance of the user's specimen at the measuring wavelength.

There is no known simple method for determining ϕ. Since all phases are then equally likely, the value of $\cos\phi$ in eq (1) can be anywhere between -1 and +1, and its expectation value is 0. Using this expectation value is equivalent to using the value $\phi = \pi/2$ in determining the threshold intensity, and the attendant uncertainty is included in the uncertainty budget.

A study was made of image profiles generated by a numerical optical model [7] of the NIST microscope system and photomasks. The model is based on the theory of partial coherence and allows variation of image formation conditions such as: linewidth; wavelength of incident radiation; transmittance and phase of the object and background illumination; and slit width. Profiles generated by this model agree very closely with profiles generated from the measurement data. Theoretical profiles were generated for lines and spaces 0.50 μm to 15 μm wide where the transmittance of the "opaque" areas is 0.2% and ϕ ranges from 0 to π The results of the study also indicate that the relative threshold intensity varied from 25% to 28% of $(I_m - I_o)$ over the range of widths simulated (figure 9). Therefore, an algorithm for determining linewidth was implemented that assumes a phase difference of $\pi/2$ and iteratively selects the threshold intensity ratio from this model-generated data according to the linewidth of the feature being measured.

5. Calibration Uncertainty of this SRM

In calibrating this standard, the positions of the geometric edges x_{edge} of the etched chrome film must be determined. The photomask is placed in a transmission-mode optical microscope with a scanning specimen stage and laser interferometer, and the image of the feature to be calibrated (*relative intensity* vs *position*) is measured [5]. The image data are obtained as an average over the central 2.55 μm along the length of the line, which effectively averages all edge irregularities along this direction, since their spatial

frequencies have been observed in SEM images to be higher than the cutoff of this sampling window. The positions of the edges are found using the mathematical model of the photomask/microscope optical system described above –starting with Maxwell's equations, artifact properties, and microscope imaging for partially coherent illumination–which predicts the intensity threshold that corresponds to the geometrical line edge. The linewidth or line center position is calculated from the positions of its edges.

5.1 Measurement uncertainty The total error of a measurement [8] is the difference between the measurement result and the true value (relative to the definition of the meter for dimensional measurements); it is the sum of systematic and random errors. The systematic error is the mean of an infinite number of measurements minus the true value; *i.e.*, the error after measurement-to-measurement variability, or measurement noise, has been removed. It is unknown and must be evaluated using all available sources of information. The random error is the result of a single measurement minus the mean of an infinite number of repeated measurements; *i.e.*, the part of the error due only to measurement-to-measurement variability.

The final measurement error is unknown because the true value is unknown (else why measure?), otherwise it could be removed from the measurement data to eliminate it. The measurement uncertainty derives from the probability distributions of the errors. The standard uncertainty is the square root of the sum of the variances of the evaluated probability distributions of the errors. It is a combination of uncertainties due to random and systematic effects, referred to as Type A and Type B uncertainty components, respectively. Measurement uncertainty is calculated as described in the ISO publication *Guide to the Expression of Uncertainty in Measurement* [9]. Type A uncertainty from the variance of the data, Type B from the variances of the probability distributions of the systematic error components. The expanded calibration uncertainty reported on the SRM certificate is 2 times the square root of the sum of the variances of all of the identified components which contribute to the measurement uncertainty. This would correspond to the 95% confidence interval if all of the uncertainty component probability distributions were Gaussian. Vendors and buyers of materials and services should use the same method for calculating measurement uncertainties.

The Type A components can be estimated directly from the measurement data. Type B uncertainty components arise from artifact imperfections and from the measurement process. In many cases only the bounds, $\pm\varepsilon$, of a Type B uncertainty component are known; in the absence of additional information its probability distribution is uniform within the bounds,

$$p(x) = 1/(2\varepsilon) \text{ for } -\varepsilon \le x \le \varepsilon, p(x) = 0 \textit{ otherwise.}$$

Then the variance u^2 and expanded uncertainty $2u$ are [9]

$$u^2(x) = \varepsilon^2/3,\ 2u(x) = 1.15\varepsilon.$$

The expanded uncertainty is greater than the bound.

The certified linewidths and pitches have separate uncertainty values because of differences in the way errors affect the measurement of widths and pitches. The values given below for uncertainty components are illustrative and typical for this calibration. Specific values are given on the accompanying calibration certificate.

5.2 Systematic effects: correlations and randomization Linewidth uncertainty arises from edge position uncertainty. If right and left edge position errors are symmetrically correlated (*e.g.*, phase of transmitted light or photometer nonlinearity), then $u(linewidth) = 2u(edge)$ and $u(pitch) = 0$. If right and left edge errors are uncorrelated (*e.g.*, chrome edge runout) then $u(linewidth) = u(edge)\sqrt{2}$.

For center-to-center pitch measurements the errors from the phase of the transmitted light and photometer nonlinearity are antisymmetrically correlated and cancel out. That is, an unknown variation of the phase, for example, will push the image of the left edge of a line to the left and the right edge to the right by the same amount, but will not displace the image of the center. This is true also for most of the edge runout error, because the average line cross section along the 2.55 μm averaging length is a trapezoid (see fig. 11) in which both edge images are affected antisymmetrically.

Substrate, structure, and air temperature vary with a dominant period of about 20 minutes. Successive measurements of each feature are at least 45 minutes apart, but usually extend overnight. The effects of temperature variation which could contribute to systematic error are effectively randomized and average to zero because the temperature is randomly distributed among the successive measurements of any feature. That is, the repeated measurements are uncorrelated with the temperature fluctuations. The resulting expanded Type A uncertainty includes all such effects and is determined directly from the data, and need not be individually evaluated. If necessary the time interval between successive measurements of a feature can be adjusted or randomized to insure decorrelation. The temperature is recorded at each measurement and no correlation has been found between temperature and measured linewidth.

It is usually advantageous to convert potential Type B uncertainties into Type A ones in this way, because the Type B can be difficult to estimate but the combined effect of all of the Type A components is measured directly.

5.3 Statistical process control Each feature on every SRM photomask is measured at least nine times over a period of at least seven hours. Type A uncertainty (commonly termed process precision) is determined directly from these repeat measurement data. One photomask linewidth SRM has been selected to be a Control photomask to serve two purposes: representative features on the Control are measured before and after every SRM calibration for statistical process control (a multivariate variance-covariance *t*-test is applied before and after each SRM calibration, see

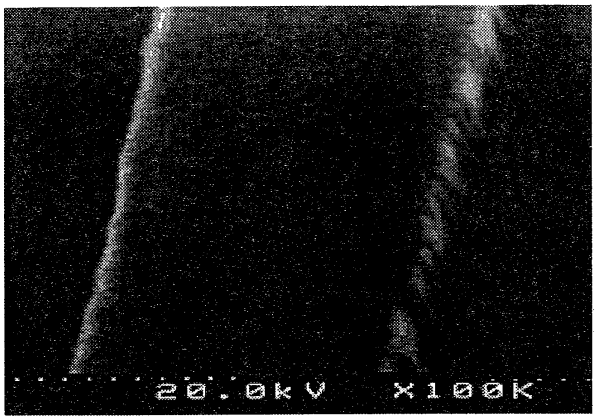

FIGURE 10. SEM micrograph showing the nonideal nature of line edges on an antireflecting-chromium photomask.

Appendix), and the pitches of several line arrays on the Control have been measured on the NIST Linescale Interferometer to provide a traceable calibration of the linewidth microscope's scale. This Control photomask is used as long as possible to accumulate a large history of measurements.

A numerical value for Type A uncertainty cannot be determined until the measuring system is operating in a state of statistical control and the source of variability is shown to be random in nature and stochastically stationary. When these criteria have been met the process standard deviation quantifies this Type A uncertainty. The value for the process precision on the certificate of calibration includes the variability of the control measurements and the variability of the nine repeated SRM measurements. The details for computing this value are given in the Appendix.

No difference is observed between long term and short term repeatability of the calibration system, and the calibrations are operator independent.

5.4 Artifact imperfections The largest components of Type B uncertainty are caused by such artifact imperfections as the irregular and sloping edges on the etched chrome (edge runout) and the unknown phase of the small amount of light transmitted through the chrome. The consequences are described briefly here and in greater detail in ref. [10]. These factors and the consequent calibration uncertainty can change from one SRM batch to the next, and are not related to the calibration system.

In the field of photomask linewidth metrology, the ideal reference standard with features which have vertical walls and smooth edges does not exist. Instead, real features have erratically varying, nonvertical edge geometries and raggedness along their length [11] (see figure 10) and resultant uncertainties of the location of the physical edge. To quantify these Type B uncertainties the feature edge geometry is examined with a scanning electron microscope. As this examination precludes use of the photomask as an SRM, only two samples from each photomask production batch are examined.

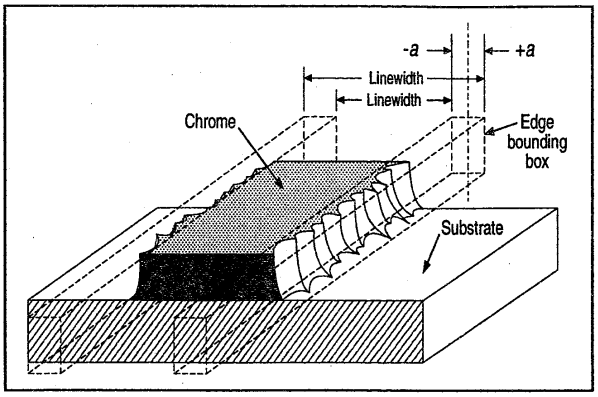

Figure 11. Schematic representation (not to scale) of a line edge as seen in an oblique view SEM micrograph. The uncertainty of linewidth measurements includes the uncertainty of the edge location resulting from nonvertical physical edge profiles. Determination of this uncertainty is accomplished by estimating the width of the box which contains 95% of all edge asperities. The edge can lie anywhere inside the box whose width is the average of such estimates made by several individuals using several different micrographs.

The SRM measurements reported represent averages over the effective length (2.55 μm) of the NIST instrument's viewing slit, positioned at the center of the line. Therefore, both the uncertainties of the edge location resulting from nonvertical edge geometry and from raggedness along the length of the line are estimated as averages along the edge of the line.

Edge waviness Several edges are examined in detail, and typically the SEM micrographs of the photomask features show that the raggedness along the length of a line is less than 30 nm and has a spatial period of 100 nm or less.**** If the user's measurements of this SRM are also averaged over a length comparable to that of the NIST viewing slit, uncertainties due to edge raggedness become insignificant (but uncertainty due to nonvertical edges remains).

Vertical edge runout The vertical edge runout (the lateral distance from the top of the chrome to the substrate at the chrome edge) is the most difficult linewidth uncertainty component to estimate, and the largest. Such subresolution features can affect the images in different microscopes and steppers in different ways [1], so the entire volume occupied by this runout must be viewed as a possible habitat of "the edge."

****Occasional isolated flaws have been observed during SEM inspection that are considerably larger than this typical edge raggedness but which are not discernable in the optical microscope at 1600 X magnification and could be present on the photomasks accepted for calibration. If the presence of such flaws in the measurement region should cause degradation of focus sharpness or of measurement precision during the calibration of a photomask, that photomask would be rejected from certification as an SRM. However, it is not known if such flaws would have any noticeable effect on the measurements.

A determination of the uncertainty caused by the nonvertical edge geometry is accomplished by estimating the width of the box containing 95% of the edge irregularities and asperities which comprise the difference between the edge location at the top surface and the corresponding edge location at the substrate level, as illustrated in figure 11. The edge is bounded by this box, and the position of the edge is considered to be anywhere inside the box with equal probability. The variance and expanded uncertainty of the edge runout are then [10]

$$u^2(x_{edge}) = (\textit{width of box}/2)^2/3, \quad (5)$$

$$2u(x_{edge}) = 1.15\ (\textit{width of box}/2) \quad (6)$$

The user is advised to examine the edge properties of the production photomasks to be measured. If the quality of the edges of the features on the user's photomasks is significantly inferior to that of this SRM, an additional level of uncertainty should be added to the uncertainty of measurements made on the user's photomasks.

Chrome transmittance The small amount of light (approximately 0.2%) which passes through the chrome interferes with the light passing around the edge and shifts the image. It has so far proved impossible to measure the phase of the light transmitted through the chrome relative to the phase of the light passing around it because of the great intensity difference, so any phase must be considered equally likely. Using eq (1) with the phase equally likely to be anywhere in the interval 0 to π, this leads to a variance in the edge position of [10]

$$u^2(x_{edge}) = 13861 \times \textit{Transmittance}, \quad (7)$$

$$2u(x_{edge}) = 235\sqrt{\textit{Transmittance}}, \text{ nm} \quad (8)$$

Because pitch measurements involve measuring the distance from one location (left edge, right edge, or center) on one feature to the same location on another feature, these edge detection errors tend to cancel and are not included in the uncertainty reported for pitch measurements.

5.5 The measurement process There are three major elements in the measurement process [12]: obtaining the microscope image data (correlating image *intensity* and *position*), analyzing the image to determine the edge intensity threshold, finding the position in the image which corresponds to that threshold. In metrology, image is everything [12]. The only factors contributing to Type B uncertainty in obtaining and measuring the microscope image are position scale inaccuracy and intensity measurement inaccuracy (photometer nonlinearity). These factors are not related to photomask quality, but can change as improvements are made to the calibration system.

Determining the edge threshold Simulating the measurement with the model reveals that the edge intensity threshold can depend on the proximity of neighboring edges, *e.g.*, on the linewidth (figure 9), since the nearest edge is often the opposite edge of the line being measured. In processing the image data, the linewidth is first estimated using the default threshold of 27%, then the correct threshold for the resulting linewidth is determined from a lookup table, and the linewidth estimated again. The process is repeated until successive thresholds converge.

Finding the edge position The digitized microscope image data are passed through a digital finite impulse response low-pass filter to remove the high frequency noise which lies beyond the spatial cutoff frequency of the microscope (mostly shot noise and vibration effects). This type of filter affects leading and trailing edges in the same way, and a cutoff frequency was chosen which has no effect on the average measured linewidth. A subset of the data near the threshold at each edge is then fit to a quadratic polynomial to interpolate between data points and further remove vibration effects. The edge is the position at which this polynomial crosses the threshold intensity.

5.6 Calibration parameters The apparatus is constructed mostly of aluminum. Some measurement parameters which affect the calibration uncertainty are:

Measurement range for linewidth	0.5 to 30 µm
Measurement range for pitch	2.0 to 70 µm
Maximum measurement time for a single feature	30 sec
Room air temperature variation (cyclic, 20 min period)	3 °C p-p
Air temperature slew rate (20 min period)	~15 mdeg/sec
Structure temperature variation (after warm-up)	~0.1 °C p-p
Structure temperature slew rate (20 min period)	~0.5 mdeg/sec
Position/intensity slope at 27% intensity, $\partial(x_{edge})/\partial I$	3 nm/%FS
Coefficient of thermal expansion, quartz	0.5×10^{-6}/ °C
Coefficient of thermal expansion, aluminum	24×10^{-6}/ °C

"p-p" means peak-to-peak; "FS" means full scale.

5.7 Calibration of the length scale Even though the scale of the linewidth microscope is a laser interferometer, it is calibrated to agree with the NIST Linescale Interferometer to remove some potential errors and to provide traceability to the meter. Several pitch patterns on the Control mask have been measured on the Linescale Interferometer. These same patterns are measured repeatedly on the linewidth microscope over a period of at least several days, extending into years. The Linescale Interferometer produces traceable pitch measurements, but is incapable of linewidth measurement.

Length scale factor When the measurement differences for each pitch (*Linescale Interferometer – linewidth microscope*) are plotted against nominal pitch for all of the patterns, the result is a straight line with noise, except for the two end points if guard lines are not used. These end points deviate from the line in opposite directions and represent proximity effects in one or both pitch measurement methods. The interior points are fitted by linear regression, resulting in a straight line with nearly zero slope. The scale factor correction for the linewidth microscope is the *slope*+1, and the scale factor uncertainty is obtained from the variance of the slope. Typically the scale factor is based on 75 or more repeated measurements on each pattern in the linewidth microscope, with a resulting slope of -0.04 nm/µm (corresponding to an implied possible cosine error of 40 µrad). This scale factor is applied to all subsequent

measurements, rendering them traceable to the NIST Linescale Interferometer.

Static temperature difference The pitches on the Control photomask were measured in the Linescale Interferometer at 20 ± 0.1 °C, while the temperature of the linewidth microscope may be different. This difference has no effect if the SRM measurement and the Control measurements which bracket it are performed at the same temperature. If they are not, the resulting error is *feature size* × *temperature difference* × *coefficient of thermal expansion (CTE) of quartz*. The maximum static temperature error is

$$\varepsilon = 70\times10^{3}\ \text{nm} \times 3\ ^{\circ}\text{C} \times 0.5\times10^{-6}/\ ^{\circ}\text{C} = 0.1\ \text{nm} \quad (9)$$

The corresponding linewidth or pitch uncertainty is

$$2u(LW\ or\ pitch) \le 1.15\ \varepsilon = 0.12\ \text{nm} \quad (10)$$

If the temperature in the user's environment differs from the temperature during calibration, the worst case error is 0.035 nm/°C.

Interferometer deadpath The interferometer deadpath is the minimum optical path length between the fixed and moving mirrors, and the metrology loop is the fixed structure which supports the mirrors and fixes their spacing. Changes in the deadpath are interpreted by the interferometer as additional measured displacement. The deadpath can change as a result of changes in the structure temperature which change the metrology loop, and changes in the index of refraction of the air. The deadpath here is about 1 cm.

The error resulting from structure temperature change is *deadpath length* × *structure temperature change* × *CTE of aluminum*. The measurement of linewidth or pitch, however, is a differential measurement in that the difference of the positions of the leading and trailing edges is determined by measuring the positions of both edges within a very short time (30 seconds for the longest pattern on this SRM); the line's width is being measured, not its position. The maximum temperature change is restricted to an interval of 30 seconds, so this maximum error becomes

$$\varepsilon = 10\times10^{6}\ \text{nm} \times 0.5\times10^{-3}\ ^{\circ}\text{C/sec} \times 30\ \text{sec} \times 24\times10^{-6}/\ ^{\circ}\text{C} = 3.6\ \text{nm}, \quad (11)$$

Since the temperature differs randomly among the repeated measurements of the same feature, this error contributes to the Type A uncertainty but its systematic effect averages to zero (sec. 5.9).

$$2u(LW\ or\ pitch) \le 4.1\ \text{nm} \rightarrow 0 \quad (12)$$

Index of refraction of air The index of refraction of air, and hence the interferometer wavelength, depends on its temperature (approximately 1 ppm/°C), pressure, and composition (relative humidity, CO_2, etc.). In this measurement system this can lead to error in two ways: the index error times the interferometer deadpath changes the apparent position in the measurement of each edge, and the index error times the measured length changes the length scale.

A deadpath error can occur if the index of refraction changes (caused, for instance, by convective turbulence) during the measurement time of 30 seconds or less. The resulting error is *deadpath length* × *air temperature change* × *change of air index of refraction/°C*,

$$\varepsilon = 10\times10^{6}\ \text{nm} \times 15\times10^{-3}\ ^{\circ}\text{C/sec} \times 30\ \text{sec} \times 1\times10^{-6}/\ ^{\circ}\text{C} = 4.5\ \text{nm}. \quad (13)$$

Since such changes are equally likely to be positive as negative, this type of error is random within the repeated measurements of a feature and is included in the measurement precision. Rapid air temperature fluctuations are averaged out during a single measurement.

$$2u(LW\ or\ pitch) \le 5.2\ \text{nm} \rightarrow 0. \quad (14)$$

If the temperature is constant but not at the nominal value of 20 °C there will be a static index of refraction error of *feature size* × *average temperature difference* × *change of air index of refraction/°C*. The worst case error for a 3 °C temperature offset is then

$$\varepsilon = 70\times10^{3}\ \text{nm} \times 3\ ^{\circ}\text{C} \times 1\times10^{-6}/\ ^{\circ}\text{C} = 0.2\ \text{nm} \quad (15)$$

$$2u(LW\ or\ pitch) \le 0.23\ \text{nm}. \quad (16)$$

An atmospheric pressure deviation of 30 mm Hg from the nominal 760 mm Hg changes the index of refraction by 9 ppm, leading to a 0.63 nm error on the longest feature

$$\varepsilon = 0.63\ \text{nm},\ 2u(LW\ or\ pitch) \le 0.72\ \text{nm}. \quad (17)$$

Deviations of the other factors affecting the index of refraction from their nominal values result in similar but much smaller random errors.

Laser polarization mixing The laser interferometer used to make these dimensional measurements is subject to a sinusoidal nonlinearity along the beam path due to polarization mixing. This leads to a maximum periodic systematic error of ~3.5 nm every one-quarter wavelength (0.16 μm) for the four beam differential interferometer used here [13]. Since repeat measurements of each photomask feature are made at substantial time intervals, thermal drift in the apparatus insures that these measurements are randomly distributed over this quarter-wavelength period. Thus this error is random, with deviations from the mean wavelength equally likely to be positive or negative, and its contribution to measurement uncertainty is included in the calculation of process precision.

Specimen and measurement axis alignment The measurement axis is the axis of the interferometer laser beam (actually the geometric center of the four beams used in this differential interferometer) and is defined as the *x*-axis. The scanning axis is the axis of motion of the piezoelectric scanning stage (or the path of the functional point, the focal point or probe, relative to the specimen), and the specimen axis is an imaginary line on the surface of the photomask perpendicular to the length of the linewidth feature being measured. Ideally these axes would coincide, but in practice it is not possible to locate these axes with great accuracy.

In this application the perpendicular distance between parallel lines (the right edge and left edge of a feature) is measured. It is important to align the specimen axis with the measurement axis, but slight misalignment of the scanning axis causes no error because only the component of motion parallel to the measurement axis is measured and this is also the component parallel to the specimen axis. In other words, a scanning axis misalignment will cause the width measurement to "slide" slightly along the length of the line, but it will always be perpendicular to the line's width. Misalignment or deviations from flatness in the interferometer mirrors can lead to errors here. These mirrors are aligned by retroreflection. If the line edges are not parallel, the average linewidth will be measured. Even though scanning axis alignment is not critical this axis is aligned as carefully as possible, first by aligning the leadscrew stage by moving it back and forth in the y direction and adjusting its rotation in the x-y plane until the interferometer indicates no periodic change in x, and then by geometrically aligning the piezoelectric stage by eye.

Misalignment of the specimen axis with the measurement axis will lead to a geometric error proportional to [1/cos(*misalignment angle*)]-1. This alignment is checked by scanning and measuring the x position of the center of the long vertical fiducial line at the right side of the pattern (see figure 3) near its top and bottom ends. The angle of rotation of the specimen can be calculated from the x positions of these centers and the nominal y distance between them. After the specimen has been mounted and aligned by eye, the alignment is checked in this way and readjusted until the computer program indicates the specimen alignment is within tolerance. The calibration program will not commence taking data unless the misalignment angle is less than ±0.1 deg. This allows a maximum cosine error of 1.5 ppm, or 0.105 nm on the longest feature on this photomask. If the specimen is tilted (*i.e.*, the specimen stage is rotated about the y-axis), the leading and trailing edges of the longer patterns will not both be in focus, and this condition will be detected in the measurements.

Abbé error A significant potential error source is the Abbé error caused by possible offset between the measurement axis and the specimen axis in combination with angular motion of the scanning stage. The measurement axis is designed to pass through the focal point of the microscope, but this is a difficult adjustment and Abbé offset in the linewidth measurement system could be as much as 1 mm. Comparison of pitch measurements made on this apparatus and on the NIST Linescale Interferometer compensate for errors of this type. Small random rotations of the scanning stage, as from bearing irregularities, may produce random errors which contribute to the measured Type A uncertainty.

5.8 Calibration of the intensity scale The microscope image intensity is measured with a photometer consisting of a photomultiplier tube (PMT), a dc amplifier, and an analog to digital converter (ADC). The PMT is placed behind a sampling aperture in the image focal plane, and connected to a 16 bit high speed ADC through a differential dc amplifier with an anti-alias RC low pass filter to remove the high frequency noise components prior to digitizing. Each line scan is bracketed by measurements of the dark voltage and appropriately corrected. The accuracy of the photometer used to measure image intensity is not an issue because only relative intensity is measured, but photometer linearity is important. Even though the photomultiplier tube is operated well below its nominal cathode voltage, some nonlinearity of response from saturation or other effects may still be present. Linewidth uncertainty components can arise from uncompensated photometer nonlinearity, and from uncertainty in the nonlinearity measurement.

An error in intensity measurement δI causes a displacement of the apparent edge of $\delta(x_{edge}) = \delta I \, \partial(x_{edge})/\partial I$. Linewidth and spacewidth can be corrected for photometer nonlinearity if it is known, or photometer readings can be linearized in real time by software if necessary. This nonlinearity can be measured with neutral density (ND) filters in a direct way, but then the uncertainty of the filter calibrations contributes to overall linewidth uncertainty. This uncertainty can be reduced by recognizing that the measured transmittance of a neutral density filter should be the same at all incident optical power levels [14]. An uncalibrated but stable ND filter can be used to determine photometer linearity.

The nonlinearity of the PMT, dc amplifier, and ADC combined can be quantified by assuming a simple nonlinear photometer model

$$v = aT + bT^2, \tag{18}$$

where $v=V/V_{FS}$ is the normalized photometer voltage when an ND filter of transmittance T is placed in front of it. There is no constant term because the dark voltage is subtracted for every measurement. Then, using no filter (T=1, v=1), and two filters with transmittances T_1 and T_2 separately, and together T_1T_2 (with corresponding normalized photometer readings v_1, v_2, v_{12}), this model gives:

$$1 = a + b \tag{19}$$

$$v_1 = aT_1 + bT_1^2 \tag{20}$$

$$v_2 = aT_2 + bT_2^2 \tag{21}$$

$$v_{12} = a\,T_1T_2 + b\,T_1^2T_2^2 \tag{22}$$

The photometer voltage is measured with no filter in place, with filter1, filter2, filter1+filter2, and an opaque filter or shutter. The photometer is accurate at T=0 and at T=1, but presents a possible error in between. These are four equations with four unknowns: a, b, T_1 and T_2. The nonlinearity can be found by solving

$$T = [-a \pm \sqrt{(a^2 + 4bv)}]/2b \text{ except for } b \text{ near } 0,$$

or

$$T \approx v/a - bv^2/a^3 + 2b^2v^3/a^5 + O(b^3) \quad \text{for } b \approx 0, \tag{23}$$

and

$$a + b = 1, \text{ and } T_1T_2/T_{12} = 1 \tag{24}$$

simultaneously for $b(v_1, v_2, v_{12})$. The solution to first order in b is

$$b = (v_{12}-v_{12}^2-2v_1v_2+v_1^2v_2+v_1v_2^2 +\sqrt{[4v_1v_2(v_1v_2-v_{12})(1-v_1-v_2+v_1v_2) - (v_{12}-v_{12}^2-2v_1v_2+v_1^2v_2+v_1v_2^2)^2]}) /2v_1v_2(1-v_1-v_2+v_1v_2). \quad (25)$$

The photometer nonlinearity is characterized by b, a perfectly linear photometer having $b = 0$, and saturation effects indicated by $b < 0$. A higher order model could be used if necessary (with additional filters), but a closed form solution may not be possible. The calculated b is very sensitive to errors in the measured v's. As a by-product, the actual filter transmittances can now be found. The voltmeter does not need to be calibrated independently because it is part of the photometer being calibrated, and only voltage ratios are measured.

Since the edge location is based on the threshold voltage, the correction to the corresponding intensity is

$$\delta T = (\textit{assumed linear } T) - (\textit{nonlinear } T) = v - T \quad (26)$$

$$= bv(v - 1)(1 + b - 2bv) \quad (27)$$

(based on the first order terms in b in the solution for T above) and the corresponding edge correction is $\delta x_{edge} = \partial(x_{edge})/\partial I\ \delta I$, where the image intensity I is identical to the filter transmittance T, since both are normalized at zero and full scale.

The photometer was calibrated *in situ*, without disassembling the microscope, in order to duplicate normal operating conditions. An ND filter with nominal transmittance of 0.55 was used for filter1 and a variable iris in the illumination path was used for filter2. This has the advantage of avoiding any possible interaction between two stacked filters due to multiple passes, and of exercising the photometer over a wider range of light levels in successive measurements of b. Several sets of values of v_1, v_2, and v_{12} were obtained with the aid of a small computer program for removing some measurement noise from the voltage readings, compensating for dark voltage with the aid of a shutter, and normalizing the voltage readings. Corresponding values of b were calculated both to 1st order and to 2nd order, with little difference in the results between the two orders.

The data indicate a mean b of about +0.02 with a larger standard deviation, implying a needed edge correction of $\delta x_{edge} \approx -1$ nm. This mean value, however, is statistically insignificant and so no photometer nonlinearity correction is required.

The dispersion of the measured values of b leads to an uncertainty in the edge caused by the variance in b:

$$u^2(x_{edge}) = (\partial(x_{edge})/\partial I)^2\ (\partial I/\partial b)^2\ u^2(b). \quad (28)$$

The slope of the *intensity/position* profile at the edge threshold intensity of ~27% is

$$\partial(x_{edge})/\partial I = 3 \text{ nm}/\% = 300 \text{ nm}, \quad (29)$$

and the expanded edge uncertainty due to photometer nonlinearity uncertainty is

$$2u(LW) = 4u(x_{edge}) = 4 \times 300\ (\partial I/\partial b)\ u(b), \quad (30)$$

$$2u(LW) = 120 \times 2u(b) = 6 \text{ nm} \quad (31)$$

Since the effects on the right and left edges of a line are correlated, the corresponding expanded linewidth uncertainty is twice the edge uncertainty.

5.9 Measurement resolution The resolution of linewidth and pitch measurements can be limited by the resolution of the interferometer used, in this case 8 nm, called the least count or least significant bit (LSB). (The intensity resolution is also limited, to 16 bits.) This could lead to a systematic error of 1/2 LSB, even in the average of any number of repeated measurements.

In this application however, the interferometer is oversampled (*i.e.*, read more frequently than the LSB would change in a noise-free environment) and digitally filtered, and –most importantly–the measurand is dithered by ambient vibration. Now the measurement resolution is limited only by the noise (the dither) and not by the interferometer. Measurement resolution can be increased through repeated measurements. Only 1 LSB peak to peak of dither is needed, in a frequency band lower than the Nyquist frequency. If the dither is higher in frequency than the microscope resolution (*spatial cutoff frequency* × *scan speed*), it can be removed from the data by filtering. The remaining (lower frequency) dither appears in the variance of the data.

Measurement in a noise-free environment would incur an added uncertainty component of 1/2 LSB arising from the resolution limit. The addition of dither and oversampling to the measurement process removes this uncertainty and replaces it with increased statistical variance, which diminishes as the number of repeated measurements increases. Even in an analog measurement, the presence of some noise can increase resolution and give confidence the system is not saturated. It is like tapping a barometer before reading the pressure.

In metrology, a little noise is a good thing.

5.10 Traceability The definition of the meter is the length of the path traveled by light in vacuum during the time interval of 1/299 792 458 of a second. This defines the speed of light in vacuum. The interval of the second is defined as the duration of 9 192 631 770 periods of the ground state hyperfine transition of *Cs*-133 [15]. The frequency of an iodine-stabilized HeNe reference laser has been measured in a manner traceable to the second. Its vacuum wavelength is then the defined speed of light divided by its frequency. The scale calibration of the of the linewidth measurement system is traceable to the NIST Linescale Interferometer [6], whose laser wavelength has been compared to the reference laser above. The wavelength in the laboratory must be corrected for the index of refraction of air, which in turn depends on the pressure, temperature, and composition of the air.

Even though the scale of the photomask linewidth measurement system is a laser interferometer, it is calibrated to agree with the NIST Linescale Interferometer to remove some potential errors and to provide traceability to the

meter. The intensity scale must be self consistent, but traceability to a unit or standard is not required.

Comparisons of the calibrated features on this SRM with other national standards laboratories show good agreement [16].

5.11 Summary All known uncertainty components and their typical values are listed in Table 1, except most of those less than 1 nm because they have no effect on the expanded uncertainty. All uncertainties are expressed as the expanded uncertainty $2U$, where $U = \sqrt{\sum variances}$ of linewidth or pitch (not of edge position), in nm [17].

The values given here are illustrative and typical for this calibration. Specific values are given in each calibration certificate. The expanded uncertainty reported on the calibration certificate has been rounded because the calculated uncertainty is only an estimate and the final few nanometers more or less should not be taken too seriously. Typically, linewidth uncertainty is less than 40 nm and pitch uncertainty is less than 10 nm.

ACKNOWLEDGMENTS

This document is based on earlier photomask SRM handbooks prepared by Carol F. Vezzetti, Ruth N. Varner, and James E. Potzick, and on the earlier SRM 474 and SRM 475 Handbooks prepared by Diana Nyyssonen and John Jerke. The Appendix was written almost entirely by Ruth N. Varner.

The photomicrographs used to examine the edge geometry were provided by the Scanning Electron Microscope Section (Sam Jones, William Keery, and Michael Postek) of the Nanoscale Metrology Group.

Many thanks to Robert Larrabee for his guidance and advice.

REFERENCES

[1] J. Potzick, "Improving Photomask Linewidth Measurement Accuracy via Emulated Stepper Aerial Image Measurement," *SPIE 14th Annual BACUS Symposium: Photomask Technology and Management*, Santa Clara, Calif., Vol. 2322-38 (Sept., 1994).

[2] D. Nyyssonen. and C. Kirk, "Optical microscope imaging of lines patterned in thick layers with variable edge geometry: theory," *J. Optical Soc. Am.*, Vol. 5 (August 1988).

[3] *1981 Annual Book of ASTM Standards*, Part 43, "Standard Practice for Preparing an Optical Microscope for Dimensional Measurements," Designation F 728-81, American Society for Testing and Materials, 1916 Race Street, Philadelphia, PA 19103.

[4] C. Croarkin and R.N. Varner, "Measurement Assurance for Dimensional Measurements on Integrated Circuit Photomasks," Natl. Bur. Stand. (U.S.) *Tech. Note 1164*, August 1982.

[5] J. Potzick, "Automated Calibration of Optical Photomask Linewidth Standards at the National Institute of Standards and Technology," *SPIE Vol. 1087, Integrated Circuit Metrology, Inspection, and Process Control*, San Jose, CA, February 1989.

[6] J. Beers, "Length Scale Measurement Procedures at the National Bureau of Standards," Natl. Bur. Stand. (U.S.), *NBSIR 87-3625*, 1987.

[7] D. Nyyssonen, "Linewidth Measurement With an Optical Microscope: The Effect of Operating Conditions on the Image Profile," *Applied Optics* Vol. 16, August 1977, pp. 2223-2230.

[8] *International Vocabulary of Basic and General Terms in Metrology*, 2nd Ed, ISO, Geneva (1993).

[9] *Guide to the Expression of Uncertainty in Measurement*, 1st Ed., ISO, Geneva (1993).

(Both available from Global Engineering Documents, 15 Inverness Way East, Englewood, Colo. 80112. 800-624-3974)

[10] J. Potzick, "Re-evaluation of the Accuracy of NIST Photomask Linewidth Standards," *Proceedings of the SPIE Symposium on Microlithography*, Vol. 2439-20, Santa Clara, Calif., pp. 232-242 (1995).

[11] D. Nyyssonen and R.D. Larrabee, "Submicrometer Linewidth Metrology in the Optical Microscope," *J. Res. Natl. Bur. Stand.* (U.S.), 92(3), May-June 1987, pp. 189-190.

[12] J. Potzick, "Accuracy in Integrated Circuit Dimensional Measurements," *Handbook of Critical Dimension Metrology and Process Control* (Kevin Monohan, Ed.), Ch. 3, Vol. CR52, SPIE, Bellingham, Wash. (1994).

[13] "High Performance Motion Control for Precision Equipment," Hewlett Packard, Co.,1990, p. 34.

[14] G. Eppeldauer, A.L. Migdall, C.L. Cromer, "Characterization of a High Sensitivity Composite Silicon Bolometer," *Metrologia*, 30, pp. 317-320 (1993)

[15] B.N. Taylor, The International System of Units (SI), NIST Special Publication 330 (1991).

[16] James Potzick, John Nunn (NPL), "International Comparison of Photomask Linewidth Standards: NPL-NIST," *Proceedings of the SPIE Symposium on Microlithography*, Vol. 2725-08, Santa Clara, Calif., (1996).

[17] B.N. Taylor and C.E. Kuyatt, "Guidelines for Evaluating and Expressing the Uncertainty of NIST Measurement Results," *NIST Technical Note 1297* (U.S. Government Printing Office, Washington, D.C., 1994).

Additional bibliography

[a] H.H. Ku, "Statistical Concepts in Metrology - With a Postscript on Statistical Graphics," Natl. Bur. Stand. (U.S.), *Spec. Publ. 747*, August 1988, p. 12.

[b] C. Croarkin, "Measurement Assurance Programs Part II: Development and Implementation," Natl.

Bur. Stand. (U.S.), *Spec. Publ. 676-II*, 1985, p. 23.

[c] J. Potzick, "Practical Photomask Linewidth Measurements," *SPIE Vol. 1261-13, Integrated Circuit Metrology, Inspection, and Process Control*, San Jose, CA, 1990.

[d] W.M. Bullis and D. Nyyssonen, "Optical Linewidth Measurements on Photomasks and Wafers," Chapter 7 in *VLSI Electronics: Microstructure Science, Semiconductor Microlithography*, Vol. 3, N.G. Einspurch, Editor, pp. 119-126 (Academic Press, New York, NY, 1982).

[e] D. Nyyssonen, "Linewidth Calibration for Bright-Chromium Photomask," *NBSIR 86-3357*, Natl. Bur. Stand. (U.S.), May 1986.

[f] J.M. Jerke, M.C. Croarkin, and R.N. Varner, "Interlaboratory Study on Linewidth Measurement for Antireflective Chromium Photomasks," Natl. Bur. Stand. (U.S.), *Special Publ. 400-74*, 1982.

Calibration Uncertainty for NIST Photomask Linewidth SRMs

serial numbers 473-B0XX

May 1998

	Uncertainty Component			Calculation	ISO Type	Value	Edge correlation factor	Expanded Uncertainty (nm) Linewidth	Pitch
Artifact	**Edge runout** The edges of the etched chrome lines when examined in a scanning electron microscope are not vertical or smooth. As the illumination wavelength in the optical measuring microscope is about five times the structure size of the line edge irregularities, these features are not fully resolved but do impart uncertainty to the measurement. If the edge position is to be characterized by a single number, then that number must have an uncertainty proportional to the nonvertical edge runout.			$2a$ = width of box containing 95% of the edge. $2u(edge) = 1.15\,a$	B	a = 17 nm	√2	27.6	0
Artifact	**Optical transmission** Since the chrome is not 100% opaque, a small amount of light leaks through it and interferes with the light transmitted and diffracted around the edges. It has so far proved impossible to measure the index of refraction of the chrome (or of a chrome/antireflecting coating), so the phase of this transmitted light relative to the light passing through the substrate is unknown, leading to uncertainty in interpreting the microscope image.			Tr = chrome transmission $2u(edge) = 235\sqrt{Tr}$	B	Tr= 0.0017	2	19.4	0
Intensity Scale	**Photometer nonlinearity**. Even though the photomultiplier tube is operated well below its normal cathode voltage, some saturation or other nonlinear effects may be possible. Slope of *intensity/position* profile $\partial(edge)/\partial I$ at threshold intensity (~27%) is 3 nm/%FS [*ie* (27±1)% intensity ⇒ *(edge* ±3) nm]. Photometer nonlinearity is measured using two ND filters and a bootstrap method, using the model *photometer voltage = a Intensity + b Intensity^2.* Edge placement error from uncompensated intensity nonlinearity δI is $\delta(edge) - \delta I\,\partial(edge)/\partial I$. Edge placement uncertainty from uncertainty in measuring nonlinearity derives from noise on the photometer voltage while using the ND filters. Right and left edges are correlated.			$\delta(edge) = \partial(edge)/\partial I \times \delta I$	B	b=0.017 δI = 0	2	0	0
Intensity Scale				$2u(edge) = \partial(edge)/\partial I \times dI/db \times 2u(b)$	A	$2u(b)$ = 0.049	2	5.9	0
Intensity Scale	**Intensity resolution** The photomultiplier voltage is amplified and sampled by a 16-bit analog-to-digital converter. Two different kinds of digital filtering, with the help of oversampling and random noise (dither) on the data, interpolate the intensity data so the resolution is high and limited only by noise.			see text	B		2	0	0
Length Scale	**Length scale traceability** A pitch standard is measured on both the NIST Linescale Interferometer and the linewidth calibration microscope.			Uncertainty of pitch standard	B	3.0 nm	1	3.0	3.0
Length Scale				Transfer to linewidth microscope	A	3.6 nm***	1	3.6	3.6
Length Scale	**Abbé error** The interferometer measurement axis is positioned to pass through the microscope focal point and to be parallel to the scan motion axis. In addition, the Abbé error is reduced through comparison with the Control photomask because low frequency rotational motion cancels out and high frequency is unlikely.			*x*-Abbé offset × yaw *y*-Abbé offset × pitch	B	Abbé offset within ±1 mm*	1	0	0
Length Scale	**Specimen cosine error** The specimen alignment is checked automatically at the beginning of each calibration sequence by measuring the *xy* positions at two points along a long fiducial line on the photomask. Measurements will not proceed if the angle is greater than 0.1 deg			$2u$ = 1.15 max(*LW* or *Pitch*) × (1/cosθ-1)	B	0.1 degree	1	0.05	0.11
Length Scale	**Interferometer cosine error** The measurement axis, the scan axis, and the specimen axis should be parallel. However, the only axis alignment which may affect the measurement is the specimen alignment described above. As long as the measurement axis is perpendicular to the line edges (specimen alignment), the scan axis alignment needs to be only approximate.			see text	B		1	0	0
Length Scale	**Laser wavelength uncertainty** removed by comparison with Control photomask.				B		1	0	0
Length Scale	**Polarization mixing** appears as random uncertainty because random thermal drift and apparatus thermal expansion between repeat measurements randomizes the distance of the interferometer mirrors along the beam over a range greater than 1/4 wavelength.				B	4 nm**	1	0	0
Length Scale	**Interferometer resolution** The interferometer is oversampled (~500 data points/μm) during the scan. Two different kinds of digital filtering, with the help of random noise (dither) on the data, interpolate the position data so the resolution is better than the native interferometer's and limited only by noise.			see text	B		1	0	0
Length Scale / Thermal	**Static** Pitch standard calibrated at different temperature from SRMs.	substrate		*(CTE quartz) × (temp diff) × (max LW or Pitch)*	B	0.2 nm*	1	0	0
Length Scale / Thermal	**Dynamic** Control and SRM measured at different temperatures.	structure deadpath		*(CTE aluminum) × (max temp change) × (deadpath)*	B	4.1 nm**	1		
Length Scale / Thermal		air deadpath		$(d\lambda/dT) \times$ *(max temp change) × (deadpath)*	B	5.2 nm**	1		
Length Scale / Thermal	**Atmospheric pressure** (dynamic)	air deadpath pressure		$(d\lambda/dP) \times$ *(max pressure change) × (deadpath)*	B	0.7 nm**	1		
	Fudge Factor	unforeseen uncertainty components			B		1	5	2
	Random	observed $2\sqrt{variance}$ of the mean of 9 or more repeated measurements (typical)***			A		1	12	9
	Combined expanded uncertainty (nm)			root sum square				**36.93**	**10.34**

* Removed by comparison with the Control photomask.

** These dynamic effects average to zero among the repeated measurements of the same feature because temperature is randomized among repeat measurements with long time intervals. They are included in the random uncertainty.

*** For illustration. Actually these random effects are combined in a different way. See Appendix.

TABLE 1. A listing of uncertainty components and their contributions to overall measurement uncertainty, in nm. Scale uncertainties are determined in a worst-case sense, *i.e.*, scale factor uncertainties (in ppm) are multiplied by the largest dimension measured. Combined random uncertainty is derived from the measurements. Combined expanded uncertainty is the root-sum-square of the uncertainty components.

APPENDIX
Process control for SRM 473 calibrations

A. Introduction

The procedures used to assure statistical control of the linewidth SRM measurement system are defined. A Control photomask with the same characteristics as the SRM photomask is used for measurement process control. Six of the features on the Control photomask are measured each time an SRM photomask is calibrated. The six features are: the nominal 0.6 μm and 5.0 μm lines from row 1; the nominal 1.0 μm and 20.0 μm lines from row 2; the nominal 6.2 pitch μm pattern from row 3; and the nominal 2.0 μm line from row 5. These correspond to features 1B, 1I, 2F, 2K, 3E, and 5B as shown on the diagram of a pattern in figure 3. The purpose of the control photomask measurements is to provide a database that can be used to determine whether or not the measurement system is in a state of statistical control. There are several factors which may cause the optical measurement system to be out-of-control. There may be a change in the measurement system or a change in environmental conditions. This document describes the initialization of the database of control measurements, use of the database to determine if the measurement system is in control, and the maintenance of the database over a long period of time.

B. Initialization of Process Parameters

When the measurement system is ready for performing SRM calibrations, a database is initialized. This database consists of at least 15 sets of repeated measurements of the six selected features on the control photomask taken over a period of several weeks [18]. This period is representative of the normal operating mode of the optical measurement system. The six features measured are identified as 1B, 1I, 2F, 2K, 3E, and 5B. These features cover the extremes of the feature sizes and the range of the feature locations on the photomask. The database includes not only the measured linewidth or spacewidth but also other pertinent information such as the date and time of the measurement, feature identification and any other potentially useful information (temperature, scan rate, etc.).

A plot of the repeated measurements for each feature, measured width or pitch versus time, is made to detect any possible anomalies in the measurement system and to verify that the system produces stable measurements whose variability is random in nature. The control database is accepted as being representative of the normal operating environment of the measurement system if no more than 5% of the measurements are suspected outliers (unexplained anomalies). If this is not the case, an effort is made to determine the cause and appropriate adjustments are made to the measurement system. The control database is then reinitialized.

The initial control database is used to estimate the mean vector (accepted mean values for each control feature) and the matrix of covariances between them. These are required elements for the multivariate Hotelling's T^2 test statistic [19]. The details for computing the estimate of the mean vector and the matrix of covariances are given below. The use of this test statistic and updating procedure for this statistic are given in following sections of this document.

From the database of control measurements for features 1B, 1I, 2F 2K, 3E, and 5B, a matrix **X** is constructed, as shown below, of the N initial repeated measurements on the control photomask. Each of the features has the same number of repeated measurements,

$$Xij = \begin{bmatrix} X_{1B,1} & X_{1B,2} & \cdots & X_{1B,N} \\ X_{1I,1} & X_{1I,2} & \cdots & X_{1I,N} \\ X_{2F,1} & X_{2F,2} & \cdots & X_{2F,N} \\ X_{2K,1} & X_{2K,2} & \cdots & X_{2K,N} \\ X_{3E,1} & X_{3E,2} & \cdots & X_{3E,N} \\ X_{5B,1} & X_{5B,2} & \cdots & X_{5B,N} \end{bmatrix} \quad \begin{array}{l} \text{where } i = 1,2,\ldots,6 \\ \text{and } j = 1,2,\ldots,N \end{array} \quad \text{(B.1)}$$

The average is computed for each of the features based on the N repeated measurements,

$$\begin{aligned} \bar{X}_{1B} &= \sum_{j=1}^{N} \frac{X_{1B_j}}{N} \quad \bar{X}_{1I} = \sum_{j=1}^{N} \frac{X_{1I_j}}{N} \\ \bar{X}_{2F} &= \sum_{j=1}^{N} \frac{X_{2F_j}}{N} \quad \bar{X}_{2K} = \sum_{j=1}^{N} \frac{X_{2K_j}}{N} \\ \bar{X}_{3E} &= \sum_{j=1}^{N} \frac{X_{3E_j}}{N} \quad \bar{X}_{5B} = \sum_{j=1}^{N} \frac{X_{5B_j}}{N} \end{aligned} \quad \text{(B.2)}$$

These values are the elements of the vector of means as denoted below:

$$\mathbf{M} = \begin{bmatrix} \bar{X}_{1B} \\ \bar{X}_{1I} \\ \bar{X}_{2F} \\ \bar{X}_{2K} \\ \bar{X}_{3E} \\ \bar{X}_{5B} \end{bmatrix} \quad \text{(B.3)}$$

A matrix is computed of the differences of the measured values minus the mean values,

$$Z_{ij} = X_{ij} - M_i, \quad \text{(B.4)}$$

where i=1,2,...,6 and j=1,2,...,N, and the variance-covariance matrix, **S**, of size 6x6, of the control database is computed with elements:

$$S_{ij} = \frac{1}{N-1} \sum_{k=1}^{N} (Z_{ik})(Z_{jk}) \quad \text{(B.5)}$$

where i=1,2,...,6 and j=1,2,...,6. The inverse of the variance-covariance matrix is computed and is used in conjunction with future control measurements to determine if the measurement system remains in a state of statistical control.

C. Procedures for Process Control

At the beginning of an SRM measurement session the features 1B, 1I, 2F, 2K, 3E, and 5B on the control mask are measured and the multivariate Hotelling's test statistic T^2 is computed as follows:

$$T^2 = \frac{N}{N+1}[\mathbf{Y} - \mathbf{M}]^T \mathbf{S}^{-1}[\mathbf{Y} - \mathbf{M}] \qquad \text{(C.1)}$$

where **Y** is a vector of newly determined widths and pitches for the above mentioned features.

The system is in control at a 95% confidence level if

$$\frac{(N-6)}{(N-1)6} T^2 \leq F_{.05}(6,\, N-6) \qquad \text{(C.2)}$$

where the $F_{.05}$ (6,*N*-6) values are found in Table 2. The value (*N*-6) corresponds to ν in Table 2.

At the end of the SRM measurement session, the control is remeasured and the test is repeated. If the system is still in control the SRM data are summarized and a certificate of calibration produced. The value of $[(N\text{-}6)/6(N\text{-}1)]T^2$ is saved in the control database and the system is ready for the next SRM measurements.

If the test indicates the system is not in control, the data are tagged when they are saved in the control database. The system is then checked to determine the cause of the test failure. A control chart may be used to determine which feature is causing the problem or to see trends in the control data. A control chart for each feature is constructed from the control database as follows. The mean, $\bar{X}$, and the standard deviation, $\hat{\sigma}$, for each feature are computed using the N repeated measurements from the control database:

$$\bar{X} = \frac{1}{N}\sum_{i=1}^{N} X_i, \text{ and } \hat{\sigma} = \sqrt{\frac{1}{N-1}\sum_{i=1}^{N}(X_i - \bar{X})^2} \qquad \text{(C.3)}$$

Control limits are computed by using the following equations:

$$\bar{\bar{X}} \pm \hat{\sigma}\, t_{.975}(N-1) \text{ for the } 2\sigma \text{ limit}$$

and (C.4)

$$\bar{\bar{X}} \pm \hat{\sigma}\, t_{.995}(N-1) \text{ for the } 3\sigma \text{ limit}$$

The values for t are found in Table 3. The value (N-1) denotes degrees of freedom, *df*, in Table 3.

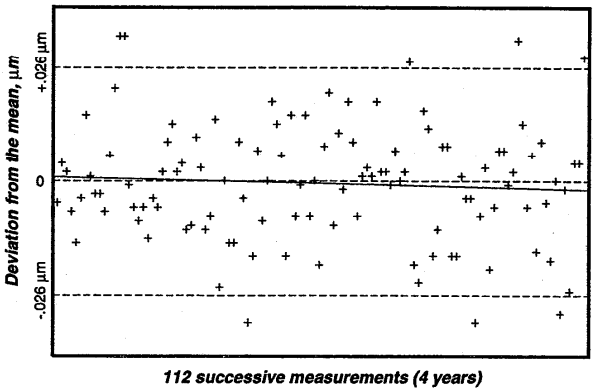

FIGURE 12. Control chart of the linewidth of feature 1B. Vertical axis is variation (µm) from the mean; horizontal axis is successive measurements. The dotted lines mark the limits of the 95% confidence level. Future measurements are added to the chart. Regression slope (solid line) implies drift of 0.7 nm/year

Figure 12 is an example of a control chart of the initial 112 measurements of feature 1B. Future measurements are added to the chart. The control limits remain the same until the process parameters are updated.

If it is determined that the cause of the failure did not affect the SRM measurements (for example, the control photomask was misaligned), the appropriate adjustments are made and the control photomask is remeasured. If the test then shows the process is in control, the SRM data are summarized, a certificate of calibration produced, and the system is ready for the next SRM measurements.

If it is determined that the cause of the failure may also have affected the SRM measurements (for example, the air-conditioning unit malfunctioned during calibration), the SRM must be remeasured after the problem has been corrected and the test indicates the system is once again in control. Major changes to the measurement system dictate reinitialization of the database.

D. Updating Process Parameters

If the measurement system remains unchanged after collecting a minimum of 30 new (good) sets of control photomask measurements, the process parameters, **M**, **S**, and $\hat{\sigma}$ are updated. Equation (B.3) is used to compute $\mathbf{M_2}$, a vector of estimated means for the recently collected control measurements; eqs (B.4) and (B.5) are used to compute $\mathbf{S_2}$, the corresponding variance-covariance matrix; and eq (C.3) is used to compute $\hat{\sigma}_2$,a vector of standard deviations for the repeated measurements for each feature. In the updating process, values that have been flagged as out of control are omitted.

Before updating the control database, a comparison is made between the two databases, the old versus the new, to determine whether or not there is a significant difference in terms of the mean vectors and the variance-covariance matrices. The equivalency of variance-covariance matrices is tested as follows:

let $l = N_1 + N_2$, (D.1)

where N_1 = number of repeated observations in the control database

and N_2 = number of repeated observations in the new set of control observations.

The new control database will contain both new and old measurements.

Let $\mathbf{S} = (N_1\mathbf{S}_1 + N_2\mathbf{S}_2)/l$ (D.2)

where $\mathbf{S}_1$ is the variance-covariance matrix of the current control database

and $\mathbf{S}_2$ is the variance-covariance matrix of additional new control measurements.

Compute the statistic [20];

$$D = 0.5N_1 \text{ trace}[(\mathbf{S}_1\text{-}\mathbf{S})^{-1}]^2 + 0.5N_2 \text{ trace}[(\mathbf{S}_2\text{-}\mathbf{S})^{-1}]^2 \quad \text{(D.3)}$$

and test whether

$$D \le \chi^2_{df}(0.05)$$

D is distributed as a chi-square random variable with df (degrees of freedom) = $0.5p(p+1)$ where $p = 6$, the number of features measured. The value of $\chi^2_{21}(0.05)$ is 32.67. If $D \le 32.67$, then the differences between the old and new covariance matrices can be attributed to random measurement error at the 95% confidence level. However, if the test fails, ($D > 32.67$), this suggests that the process has changed in some manner and the cause needs to be identified and evaluated. If the change is significant, appropriate action must be taken and the control process re-initialized.

If the covariance matrices are statistically the same, the means are compared. To do this, first a pooled covariance matrix is computed:

$$\mathbf{S_p} = [(N_1\text{-}1)\mathbf{S}_1 + (N_2\text{-}1)\mathbf{S}_2]/(l - 2) \quad \text{(D.4)}$$

where $\mathbf{S}_1$ and $\mathbf{S}_2$ are defined in (D.2).

Then the statistic is computed:

$$T^2 = \frac{N_1 N_2 (l-p-1)}{lp(l-2)}[\mathbf{M_1} - \mathbf{M_2}]^T \mathbf{S}_P^{-1}[\mathbf{M_1} - \mathbf{M_2}]$$

(D.5) and tested whether:

$$T^2 \le F_{.05}(p, l\text{-}p\text{-}1)$$

where N_1, N_2 and l are defined in (D.1),

$\mathbf{M}_1$ is the mean vector for the current database,

$\mathbf{M}_2$ is the mean vector for the newly collected control data,

and $p = 6$, the number of measured features.

T^2 is a random variable with an F-distribution with p degrees of freedom in the numerator and with l-p-1 degrees of freedom in the denominator. The $F_{.05}(p, l\text{-}p\text{-}1)$ value is given in Table 2. If $T^2 > F_{.05}(p, l\text{-}p\text{-}1)$, this suggests that there has been a change in the measurement process. The change needs to be identified and appropriate action needs to be taken to re-establish the measurement system and begin the process control anew. However, if $T^2 \le F_{.05}(p, l\text{-}p\text{-}1)$ then the differences between the old and new mean vectors can be attributed to measurement error at the 95% confidence level. Since the test for equality of means was only performed if the hypothesis of equal covariance matrices was not rejected, it can be said that there has been no statistically discernible change in the measurement process at the 90% confidence level and the control may be updated to include the new measurements. The covariance matrix is updated as shown in eq (D.4) and the current covariance matrix is

$$\mathbf{S} = \mathbf{S_P} \quad \text{(D.6)}$$

The mean vector is updated as shown below:

$$\mathbf{M} = \frac{N_1\mathbf{M_1} + N_2\mathbf{M_2}}{N_1 + N_2} \quad \text{(D.7)}$$

The standard deviation for each feature is updated as follows:

$$\hat{\sigma} = \sqrt{\frac{(N_1 - 1)\hat{\sigma}_1^2 N_1 + (N_2 - 1)\hat{\sigma}_2^2 N_2}{N_1 + N_2 - 2}} \quad \text{(D.8)}$$

E. Uncertainty Statement for SRM 473

The uncertainties for the certified linewidth and pitch values given in the certificate include small contributions from the Type A uncertainty (measurement precision) and a contribution from the Type B uncertainty. The Type B uncertainty for both pitch and linewidth values includes a length dependent contribution introduced by correcting the measurements to agree with the NIST Line Scale Interferometer measurements (see sec.5.7). The Type B uncertainty for the linewidth values has a significant contribution (on the order of 0.03 μm to 0.04 μm) resulting from the edge geometry of the features. See Table 1 for a detailed summary of uncertainty components.

Before determining the total uncertainty for the reported certificate values, it is assumed that all the measurements on the SRM and in the control database have been corrected to compensate for the difference of measurements between the NIST Line Scale Interferometer System and the optical linewidth measurement system. The correction factor is derived by using the model given below and ordinary least squares to estimate α and its variance:

$$X = \alpha Y + \varepsilon \quad \text{(E.1)}$$

where X represents a measurement from the linewidth measurement system,

Y represents a measurement from the linescale measurement system,

and ε is the random error of measurement.

Then the uncertainties, U_{LW} and U_P, for linewidth and pitch measurements are determined by the equations below:

The variance of each SRM measurement is

$$\hat{s}_j^2 = \bar{x}_j^2 \frac{\text{var}(\hat{\alpha})}{\hat{\alpha}^2} \frac{1}{n-1}\sum_{i=1}^{n}(x_i - \bar{x}_j)^2 \quad \text{(E.2)}$$

where x_j is the average of the jth feature,

$\text{var}(\hat{\alpha})$ is the estimated error of the slope,

$\hat{\alpha}$ is the least squares determination of the slope,

and n is the number of repeated measurements.

The variance of the control measurements is

$$\hat{\sigma}_k^2 = \bar{c}_k^2 \frac{\text{var}(\hat{\alpha})}{\hat{\alpha}^2} + CV_k \quad \text{(E.3)}$$

where

$\bar{c}_k$ is the average of the kth control feature

and CV_k is the kth diagonal element of the variance- covariance matrix for the control data.

Then the pooled variance from the N repeated measurements in the control database and the n repeated measure-

ments of the SRM is

$$\hat{s}_p^2 = \frac{(N-1)\sum_{k=1}^{p}\hat{\sigma}_k^2 + (n-1)\sum_{j=1}^{q}\hat{s}_j^2}{(N-1)p + (n-1)q} \qquad \text{(E.4)}$$

The uncertainty for pitch measurements is

$$U_P = 2\sqrt{[s_p^2/n + \Sigma(\textit{Type B uncertainty variances})]}$$

and the uncertainty for linewidth measurements is

$$U_{LW} = 2\sqrt{[s_p^2/n + \Sigma(\textit{Type B uncertainty variances})]}$$

where s_p is determined by using eqs (E.2), (E.3), and (E.4) for pitch and linewidth measurements on the SRM and in the control database. Typically s_p = 015 μm and n = 9 repeat measurements. The factor 2 is the NIST expansion factor [17].

APPENDIX ACKNOWLEDGMENTS

The authors thank Susannah Schiller for suggesting the statistical tools to assure process control of the linewidth SRM measurement system.

APPENDIX REFERENCES

[18] Croarkin, C., *Measurement Assurance Programs Part II: Development and Implementation*, Natl. Bur. Stand. (U.S.) Spec. Publ. 676-II, 1985, p. 35.

[19] Anderson, T.W., *An Introduction to Multivariate Statistical Analysis*, 2nd ed. John Wiley and Sons, 1984. Chapter 5, pp. 156-190.

[20] *ibid.*, p. 423.

Table 2

Critical Values of $F_{.05}(6,\nu)$ of the F-Distribution

ν	$F_{.05}(6,\nu)$	ν	$F_{.05}(6,\nu)$	ν	$F_{.05}(6,\nu)$
10	3.217	48	2.295	86	2.206
12	2.996	50	2.286	88	2.203
14	2.848	52	2.279	90	2.201
16	2.741	54	2.272	92	2.199
18	2.661	56	2.266	94	2.197
20	2.599	58	2.260	96	2.195
22	2.549	60	2.254	98	2.193
24	2.508	62	2.249	100	2.191
26	2.474	64	2.244	102	2.189
28	2.445	66	2.239	104	2.187
30	2.421	68	2.235	106	2.185
32	2.399	70	2.231	108	2.184
34	2.380	72	2.227	110	2.182
36	2.364	74	2.224	112	2.181
38	2.349	76	2.220	114	2.179
40	2.336	78	2.217	116	2.178
42	2.324	80	2.214	118	2.176
44	2.313	82	2.211	120	2.175
46	2.304	84	2.209	∞	2.099

Table 3

Critical Values of $t_{.975}(df)$ and $t_{.995}(df)$ of the Student's t-Distribution

df	$t_{.975}$	$t_{.995}$	*df*	$t_{.975}$	$t_{.995}$
10	2.228	3.169	66	1.997	2.652
12	2.179	3.055	68	1.995	2.650
14	2.145	2.977	70	1.994	2.648
16	2.120	2.921	72	1.993	2.646
18	2.101	2.878	74	1.993	2.644
20	2.086	2.845	76	1.992	2.642
22	2.074	2.819	78	1.991	2.640
24	2.064	2.797	80	1.990	2.639
26	2.056	2.779	82	1.989	2.637
28	2.048	2.763	84	1.989	2.636
30	2.042	2.750	86	1.988	2.634
32	2.037	2.738	88	1.987	2.633
34	2.032	2.728	90	1.987	2.632
36	2.028	2.719	92	1.986	2.630
38	2.024	2.712	94	1.986	2.629
40	2.021	2.704	96	1.985	2.628
42	2.018	2.698	98	1.984	2.627
44	2.015	2.692	100	1.984	2.626
46	2.013	2.687	102	1.983	2.625
48	2.011	2.682	104	1.983	2.624
50	2.009	2.678	106	1.983	2.623
52	2.007	2.674	108	1.982	2.622
54	2.005	2.670	110	1.982	2.621
56	2.003	2.667	112	1.981	2.620
58	2.002	2.663	114	1.981	2.620
60	2.000	2.660	116	1.981	2.619
62	1.999	2.657	118	1.980	2.618
64	1.998	2.655	120	1.980	2.617
			∞	1.960	2.576

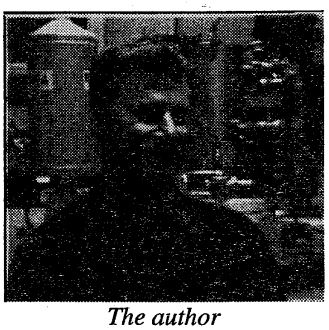

The author

☆U.S. GOVERNMENT PRINTING OFFICE: 1997 - 423-969/60047